Molecular Imaging in Cardiology

17

Almost all aspects of life are engineered at the molecular level, and without understanding molecules we can only have a very sketchy understanding of life itself.

Francis Harry Compton Crick

17.1 The Clinical Problem

Coronary artery disease (CAD), stroke, and congestive heart failure (CHF) are responsible for the majority of all cardiovascular deaths. The current major diagnostic imaging procedures in nuclear cardiology to address the issues of CAD and heart failure are based on the assessment of myocardial blood flow (MBF) and substrate metabolism using FDA approved SPECT and PET radiopharmaceuticals (Table 17.1). A number of review articles have extensively discussed various clinical issues and the relative significance of noninvasive imaging techniques in nuclear cardiology (Schwaiger and Bengel 2003; Machac 2005; Berman et al. 2007).

In the last 30 years, the application of qualitative perfusion imaging based on SPECT has been extended to allow for the combined evaluation of perfusion, perfusion reserve, and ventricular function. With PET, however, quantitative assessment of perfusion has become possible. In combination with pharmacological stress agents, the coronary flow reserve (CFR) can be quantitatively assessed as an early marker of endothelial dysfunction. Unfortunately, perfusion imaging often identifies the disease process after it is well established and has caused significant damage. Since many patients with CAD do not have angina, the majority of patients undergoing perfusion imaging may have advanced disease at the initial diagnosis. It is important to define the CAD process early, when therapeutic interventions to prevent clinical manifestations may be more appropriate. PET in combination with metabolic tracers has become an important clinical marker for the ischemically jeopardized myocardium. FDG-PET is widely considered as the gold standard for tissue viability in the management of patients with advanced CAD and impaired left ventricular function (LVF). Radiolabeled catecholamine analogues, such as MIBG and HED, provide visualization of sympathetic nerve terminals that are functionally altered in patients with diabetes mellitus and cardiomyopathy. These procedures, however, have not been approved by the FDA for routine clinical diagnostic use.

In cardiology, a paradigm shift is taking place with the emphasis from treatment to prevention of the disease. Current strategies involve the use of targeted markers of biological processes. With the recent advances in molecular biology, including genomics and proteomics, molecular imaging using biologically targeted radiopharmaceuticals (Table 17.2) will play a key role in this interdisciplinary approach to understanding the origins, pathogenesis, and progress of cardiac diseases, and in evaluating therapeutic interventions. These include novel imaging strategies for CAD, vulnerable

Table 17.1 FDA approved PET and SPECT radiopharmaceuticals in cardiology

Indication	SPECT	PET
Myocardial blood flow	^{201}Tl-chloride	[^{13}N]NH_4^+
	^{99m}Tc-Sestamibi (Cardiolite™)	^{82}Rb chloride
	^{99m}Tc-Teboroxime (Cardiotec™)	
	^{99m}Tc-Tetrofosmin (Myoview™)	
Blood pool	^{99m}Tc-RBC or HSA	
Infarction	^{99m}Tc-PYP	

S. Vallabhajosula, *Molecular Imaging: Radiopharmaceuticals for PET and SPECT,*
DOI: 10.1007/978-3-540-76735-0_17, © Springer-Verlag Berlin Heidelberg 2009

Table 17.2 Molecular imaging in nuclear cardiology

Indication	Biological process	SPECT RP	PET RP
Blood flow	Myocardial perfusion		$[^{15}O]$Water $[^{13}N]NH_4^+$ ^{82}Rb chloride ^{18}F-BMS-747158-02 ^{62}Cu-PTSM or ETS
Metabolism	Oxygen		$[^{15}O]O_2$ $[^{11}C]$Acetate
	Glucose		$[^{18}F]$FDG
	Free fatty acids	^{123}I-BMIPP	$[^{18}F]$FTHA
Neurotransmission	Presynaptic –adrenergic	^{123}I-MIBG	$[^{11}C]$HED $[^{18}F]$Metaraminol
	Adrenoreceptors		$[^{11}C]$CGP-12177
Angiogenesis	$\alpha_v\beta_3$ integrin	^{111}In-VEGF$_{121}$	^{18}F or ^{64}Cu-RGD
Atherosclerosis	Macrophages		$[^{18}F]$-FDG
Apoptosis	PS expression	^{99m}Tc-HYNIC-Annexin V	^{18}F-Annexin V ^{64}Cu-DOTA-Annexin V

plaque, atherothrombosis, angiogenesis, heart failure, apoptosis, stem cell transplantation, and gene therapy (Schwaiger and Bengel 2003; Strauss et al. 2004; Jaffer and Weissleder 2004; Dobrucki and Sinusas 2005; Wu et al. 2007; Sanz and Fayad 2008). The major goals of molecular imaging techniques in nuclear cardiology are (a) earlier detection of the disease, (b) objective monitoring of therapies, and (c) better prognostication of the disease progression.

17.2 Pathophysiology

The coronary arteries originate from the left and right coronary sinuses of the aorta (Fig. 17.1). The left main coronary artery divides into two major arteries: the left anterior descending artery (LAD) and the left circumflex artery (LCx). The right coronary artery (RCA) divides into a posterior descending artery (PDA) and a posterior left ventricular branch. The cardiac muscle has two essential properties: electrical excitability and contractility. The ability of myocardial muscle cells to contract and generate the force necessary to maintain blood circulation is achieved through the unique contractile function of two proteins of the sarcomere (actin and myosin) of the syncytially arranged myocardial fibers. Also, the heart muscle has a rich supply of the high-energy phosphates needed for the contraction.

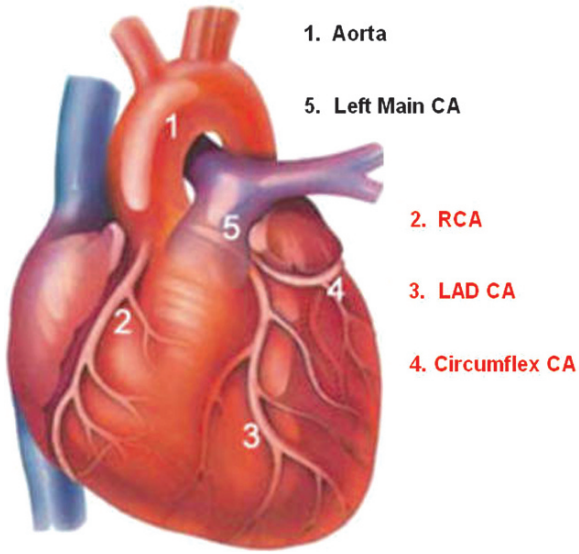

Fig. 17.1 Heart with coronary arteries

17.2.1 Coronary Artery Disease

The majority of patients with acute coronary syndromes (ACS) present with unstable angina, acute myocardial infarction, and sudden coronary death. The disease may be asymptomatic until advanced in severity or complications. CAD is an immune inflammatory process, which, over decades, results in arterial narrowing (Ross 1999; Libby 2002). Atherosclerosis is a

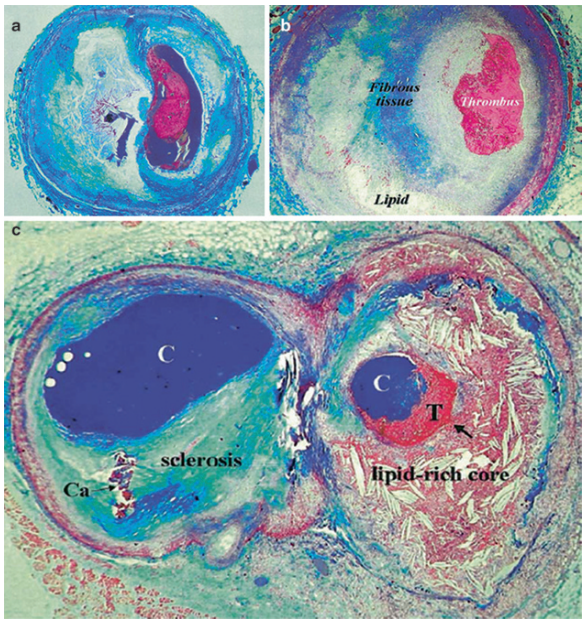

Fig. 17.2 Atherosclerosis and thrombosis in coronary arteries (CA): (**a**) Cross-sectioned CA containing a ruptured plaque with a nonocclusive platelet-rich thrombus superimposed; (**b**) Cross section of a CA containing a stenotic atherosclerotic plaque with an occlusive thrombosis superimposed (plaque erosion); (**c**) Atherothrombosis: a variable mix of chronic atherosclerosis and acute thrombosis. Cross-sectioned arterial bifurcation illustrating a collagen-rich (*blue-stained*) plaque in the circumflex branch (*left*) and a lipid-rich and ruptured plaque with a nonocclusive thrombosis superimposed in the obtuse branch (*right*). C = contrast in the lumen; Ca = calcification; T = thrombosis. (Fuster et al. 2005)

systemic disease with focal manifestations, and it is by far the most frequent underlying cause of CAD. It is also is a complex disease in which cholesterol deposition, inflammation, and thrombus formation play a major role. Atherosclerotic lesions (Fig. 17.2), according to the American Heart Association classification with recent modifications are divided into two groups: nonatherosclerotic intimal lesions and progressive atherosclerotic lesions (Spagnoli et al. 2007). A third group of lesions, healed atherosclerotic plaques, are the most prevalent lesions, particularly in the carotid arteries. A variety of factors contribute to the development and progression of atherosclerosis. Dysfunction of the endothelium, which maintains vascular homeostasis by regulating vascular tone, smooth muscle cell proliferation, and thrombogenicity, is thought to be the earliest step in the development of CAD. The endothelial dysfunction results in the imbalance of vascular regulatory mechanisms to cause damage to the arterial wall. Inflammation, macrophage infiltration, lipid deposition, calcification, extracellular matrix digestion, oxidative stress, cell apoptosis, and thrombosis are among other molecular mechanisms that contribute to plaque development and progression (Libby 2002; Falk 2006; Virmani et al. 2006). Atherosclerosis, alone, is rarely fatal; it is thrombosis, superimposed on a ruptured or eroded atherosclerotic plaque, that precipitates the life-threatening clinical events, such as acute coronary syndromes (ACS) and stroke (Falk 2006). Therefore, the term atherothrombotic disease is more appropriate since the atherosclerotic and the thrombotic processes are interdependent (Fuster et al. 2005).

17.2.1.1 Vulnerable Plaque

Since the 1970s, scientists have sought to find the mechanisms responsible for converting chronic coronary atherosclerosis to acute coronary artery disease. Despite major advances in the treatment of coronary heart disease patients, a large number of victims of the disease, who are apparently healthy, die suddenly without prior symptoms. In the 1990s the term *vulnerable plaque* was introduced to describe the rupture prone plaques as being the underlying cause of most clinical coronary events (Muller et al. 1994). Based on histopathological observations, a nonthrombosed lesion, that most resembles the acute plaque rupture, has been identified as the thin cap fibroatheroma (TCFA), which is characterized by a necrotic core with an overlying fibrous cap measuring <65 μm, containing rare smooth muscle cells and numerous macrophages (Fig. 17.3) (Falk 2006; Virmani et al. 2006). An inflamed TCFA is suspected to be a high risk/vulnerable plaque (Muller et al. 2006).

Stable plaques are characterized by intimal thickening associated with lipid deposition, a chronic inflammatory infiltrate, but without evidence of necrosis, whereas vulnerable and ruptured plaques are characterized by an "active" inflammation involved in the thinning of the fibrous cap, predisposing the plaque to rupture (Spagnoli et al. 2007). Since rupture-prone plaques are not the only vulnerable plaques, it was proposed that all types of atherosclerotic plaques, with high likelihood of thrombotic complications and rapid progression, should be considered as vulnerable

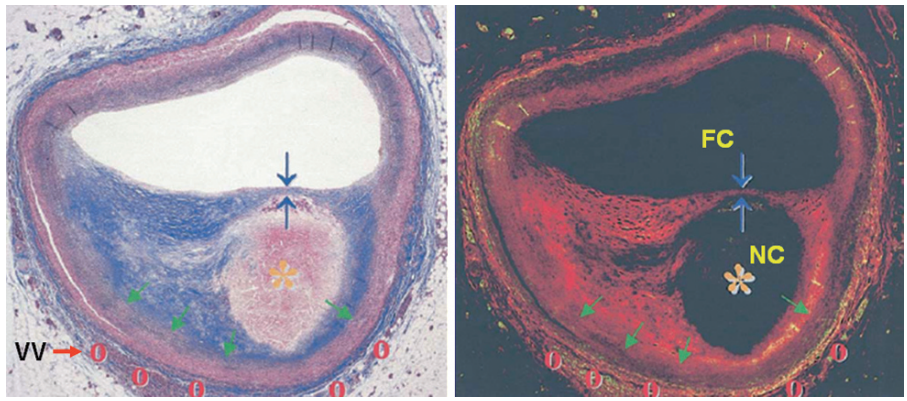

Fig. 17.3 Vulnerable Plaque: cross section of a coronary artery containing plaque assumed to be rupture-prone containing a large lipid-rich necrotic core (NC), thin fibrous cap (FC), expansive remodeling (*green arrow*), and vasa vasorum and neovascularization (VV) (Falk 2006)

plaques. In addition, since the vulnerable blood (prone to thrombosis) and vulnerable myocardium (prone to fatal arrhythmia) play an important role in the clinical outcome, the term "vulnerable patient" has been regarded as being more appropriate (Naghavi et al. 2003).

17.2.1.2 Myocardial Infarction

Myocardial infarction (MI) occurs in the setting of an acute coronary vessel occlusion, with a variable amount of spasm, and increased myocardial demand as contributing factors. Most of the ACS are thought to be the result of sudden luminal thrombosis which occur from three different pathologies: plaque rupture, erosion, and calcified nodules (Virmani et al. 2006). Histopathological studies reveal a large peripheral zone infiltrate by neutrophils that surround the subendocardial central zone devoid of neutrophils. The peri-infarct zone is a complex collection of regions in different states of injury, depending on the amount of blood flow reduction, myocardial metabolic demand, and the rate of onset and duration of the blood flow reduction. Myocardial necrosis and severe acute ischemia lead to increased permeability, cell membrane disruption, and leakage. Different myocardial tissue states or zones, such as hibernating and stunned myocardium, may be present depending on the extent of damage, viability and function (Travin and Bergmann 2005). The hibernating myocardium is the term applied to a dysfunctional myocardium with reduced perfusion (ischemia) at rest, but preserved cell viability.

17.2.2 Congestive Heart Failure

CHF stems from inadequate cardiac output, due to systolic or diastolic left ventricular function. The primary causes are ischemic heart disease and hypertension. Both, idiopathic cardiomyopathy (ICM) and ischemic cardiomyopathy (ISM) are widespread and are major underlying cardiac diseases responsible for heart failure. Besides the risk of sudden cardiac death, patients with CHF can have intraventricular dyssynchrony (or left bundle branch block), which causes the two ventricles to beat in an asynchronous fashion, reduces systolic function, and increases systolic volume. Autonomic dysfunction has been shown to increase the risk of death in patients with heart disease and may be applicable to all patients with cardiac disease, regardless of etiology (Barron and Lesh 1996). The impaired cardiac presynaptic function has pathophysiological implications in the occurrence of lethal cardiac events in patients with heart failure.

The autonomic innervation of the heart is the primary extrinsic control mechanism regulating cardiac performance. The heart is innervated by the parasympathetic and sympathetic nerve fibers. The left ventricle of the heart is primarily supplied by sympathetic nerves that modify cardiovascular performance in adapting to the changing hemodynamic requirements. The parasympathetic nervous system primarily innervates the atria and the conduction system. The major neurotransmitters of the sympathetic and parasympathetic systems are norepinephrine and acetylcholine, which define the stimulatory and inhibitory physiological effects of each system. There is a highly regulated balance in the sympathetic and parasympathetic input to optimize cardiac performance.

17.3 Radiopharmaceuticals in Nuclear Cardiology

The conventional imaging procedures in nuclear cardiology have focused on obtaining physiologic or metabolic information in the diagnostic and prognostic evaluation of cardiovascular diseases (Table 17.1). In the near future, several molecular imaging approaches will become important adjuncts to the clinical management of patients with CAD and heart failure. These techniques may offer the potential to directly track biochemical processes and signaling events that precede the pathophysiological changes. The basic principles involved in the development of targeted biological markers of molecular and physiological processes are briefly discussed.

17.3.1 Myocardial Blood Flow

MBF is regulated by anatomical, hydraulic, mechanical and metabolic factors. Autoregulation of MBF is driven by changes in regional myocardial metabolism and oxygen consumption. Under resting conditions, MBF is one fifth the maximum flow capacity, which occurs during reactive hyperemia and, or with maximum pharmacological vasodilation (Sinusas and Zaret 1995). Near-maximal MBF can be produced by intense metabolic stress associated with exercise. The difference between the peak and basal MBF represents the coronary flow reserve (CFR), which is reduced in the presence of severe CAD.

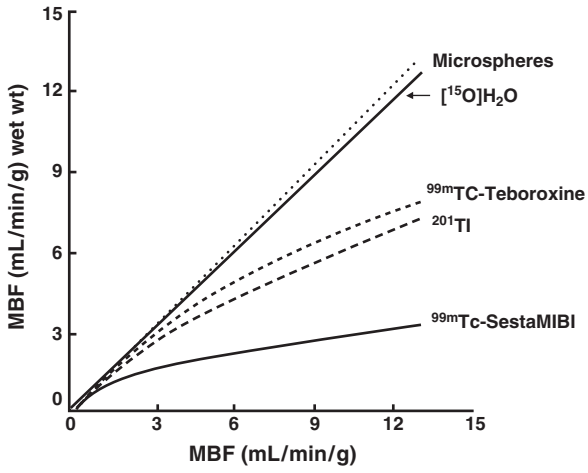

Fig. 17.4 Correlation between the measured MBF based on imaging studies and the expected MBF

The resting MBF is not reduced until the stenosis exceeds 90% of the normal vessel diameter. The coronary flow reserve, however, is reduced with only a 50% diameter stenosis (Gould et al. 1974). Therefore, myocardial perfusion imaging (MPI) is performed in conjunction with exercise or pharmacological vasodilatation (using adenosine, dipyridamole, or dobutamine) in order to identify subcritical coronary stenosis. MPI maps the relative distribution of coronary flow, which is normally almost uniform in the absence of prior infarction or fibrosis.

17.3.1.1 PET Radiotracers for Perfusion

Several radiopharmaceuticals are available for evaluating the relative distribution of MBF based on SPECT or for measuring regional MBF in absolute quantitative units (mL/min/g) based on PET.

The ideal flow tracer accumulates in, or clears from, the myocardium linear in proportion to MBF. The relationship between uptake and clearance of the radiotracer and MBF should be constant and independent of MBF, physiological and pathological changes of the myocardial tissue state, and the myocardial metabolism. Most radiotracers used for imaging the myocardial perfusion/blood flow, however, do not fully meet these requirements (Schelbert 2004).

As described previously (Chap. 16), the first pass unidirectional extraction fraction E is the fraction of the tracer that changes across the capillary membrane during a single transit of tracer bolus through the coronary circulation. For most diffusible radiotracers, such as [^{15}O]water, $E < 1$ declines with increasing MBF. The relationship between E and the permeability-surface product and blood flow is described by Renkin and Crone. It is also important to note that the E for radiotracers administered as bolus is generally higher than the steady state extraction fraction, also called the extraction ratio (Schelbert 2004). Also, the first pass retention fraction R of the radiotracer may decrease at higher flow rates due to back diffusion of the radiotracer into the vascular space and blood. The plot of the myocardial net uptake ($E \times F$) for several radiotracers, as a function of MBF (Fig. 17.4), suggests that the net uptake would increase linearly with higher blood flows,

but correlates nonlinearly with blood flow, except for [^{15}O]water.

[^{15}O]water meets the criteria for an ideal radiotracer for MBF measurement most closely. Based on a single tissue compartment model, MBF (mL min^{-1} g^{-1}) estimates in normal human subjects are 0.90 ± 0.22 at rest and 3.55 ± 1.15 with stress, based on intravenous dipyridamole (Schelbert 2004).

[^{13}N]Ammonia (NH_3) in circulation exists predominantly as an ammonium ion NH_4^+ at normal pH. It may be actively transported into the myocardial cells via the Na^+/K^+ pump or by the passive diffusion of neutral lipid soluble ammonia. Inside the cell, ammonia is quickly converted to ammonium ion which is rapidly converted and trapped as glutamine by the enzyme *glutamine synthase* (Schelbert 2004). Because of the large intracellular levels of glutamine, the washout of N-13 activity from the cell is minimal. Since the rate of their back-diffusion depends on MBF, the retained fraction *R* declines with higher flow.

Intrasubject comparison studies have demonstrated a close linear correlation between MBF estimates determined by [^{15}O]water and [^{13}N]ammonia techniques, over a range of flows from 0.5–5.0 mL min^{-1} g^{-1} (Nitzsche et al. 1996). Also, global and regional MBF estimates with [^{13}N]ammonia have shown a close correlation to MBF estimates which were determined based on the inert argon gas washout technique (Kotzerke et al. 2001). In patients with CAD and previous myocardial infarctions, MBF estimates with [^{13}N]ammonia and [^{15}O]water may markedly differ in regions of previously infracted myocardium (Schelbert 2004). MBF imaging with [^{13}N]ammonia-PET, demonstrating anterior and lateral defects, is shown in Fig. 17.5.

$^{82}Rb^+$ as a K^+ analog, is actively transported into the myocardial cells via the Na^+/K^+ pump. The extraction fraction decreases at high flows and can be altered by drugs, severe acidosis, hypoxia and ischemia. $^{82}Rb^+$ appears to leak from the irreversibly injured myocardium, but is retied or continues to accumulate in only reversibly injured myocardium (Schelbert 2004). In normal subjects, at base line, and with dipyridamole stress, there is a close correlation between MBF estimates with $^{82}Rb^+$ and [^{15}O]water (Lin et al. 2001). An example of ^{82}Rb-PET images showing relatively normal perfusion (Machac 2005) is provided in Fig. 17.6.

^{62}Cu-PTSM is a lipophilic Cu(II) complex that can diffuse across the cell membrane. Following reduction by the sulfhydryl groups, copper binds to intracellular proteins and is trapped in the myocardium. While

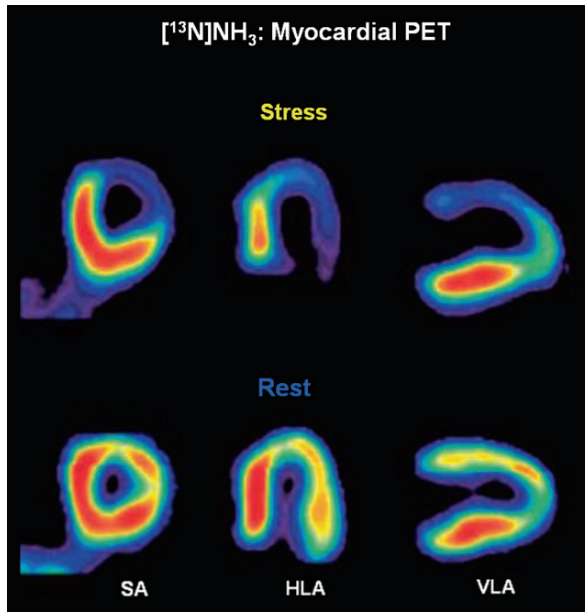

Fig. 17.5 Myocardial blood flow imaging with [^{13}N]ammonia-PET demonstrating anterior and lateral defects during pharmacological stress and significant improvement at rest, consistent with ischemia. SA, short axis; HLA, horizontal long axis; VLA, vertical long axis (Machac 2005)

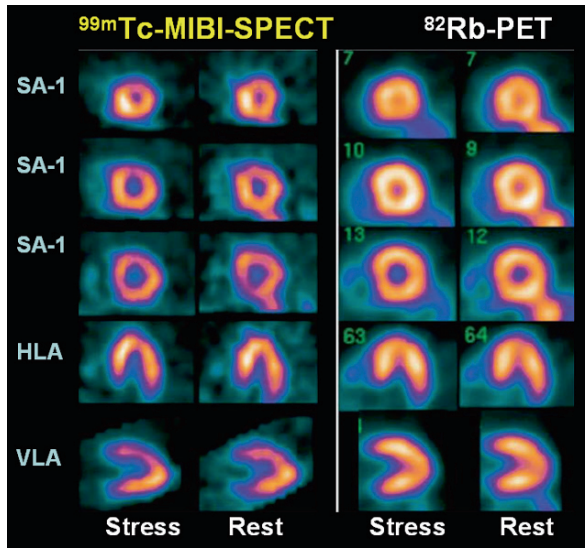

Fig. 17.6 Comparison of Myocardial SPECT and PET: ^{99m}Tc sestamibi dipyridamole stress and rest images show a mild-to-moderate anterior wall defect at stress with a suggestion of partial improvement at rest, while the ^{82}Rb-PET images shows normal perfusion (Machac 2005)

Cu-PTSM has demonstrated significant potential for imaging myocardial blood flow, very high binding to albumin in circulation impairs its ability for quantitative

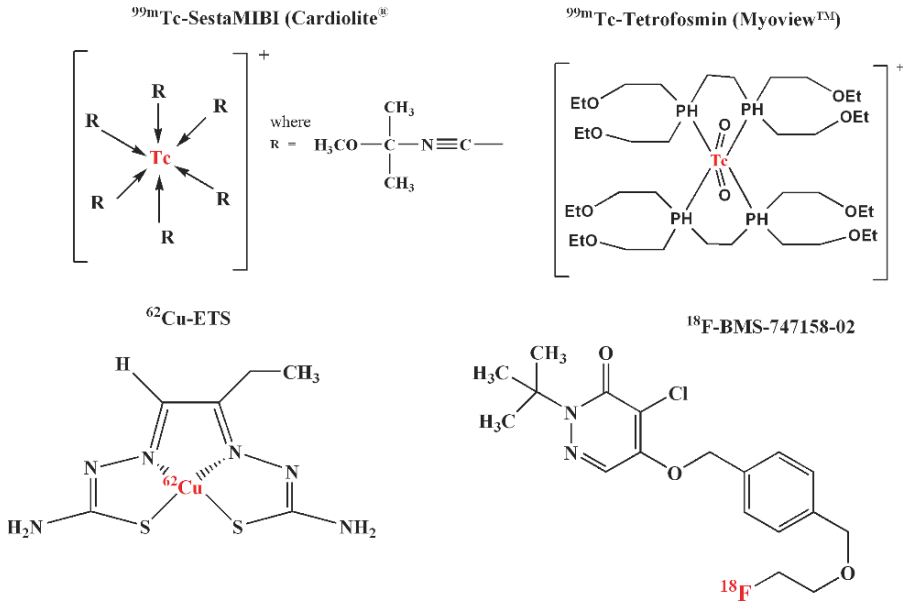

Fig. 17.7 SPECT and PET radiopharmaceuticals for imaging myocardial perfusion

determination of myocardial perfusion (Basken et al. 2008). A second generation of the Cu-BTS complex known as ^{62}Cu-ETS (Fig. 17.7), with minimal plasma protein binding, is under clinical evaluation.

Recently, the first ^{18}F-labeled radiopharmaceutical for the assessment of myocardial perfusion was proposed. More specifically, [^{18}F]fluorobenzyl triphenyl phosphonium (^{18}F-BMS-747158-02) (Fig. 17.7), a member of the class of potentiometric lipophilic phosphonium cations originally developed for the measurement of the mitochondrial membrane potential, was introduced for myocardial perfusion imaging (Madar et al. 2006). The accumulation of this tracer depends primarily on the mitochondrial membrane potential. Furthermore, the myocardium-to-liver uptake ratio is approximately one, hampering image contrast for myocardial structures (Huisman et al. 2008). Based on preclinical studies, it has been observed that a high and flow-independent first-pass extraction fraction promises linearity between tracer uptake and myocardial blood flow.

17.3.1.2 SPECT Radiotracers for Perfusion

^{201}Tl as thallous chloride behaves like a K^+ analogue and is highly extracted by the myocardial cell. It was first introduced in the 1970s as a radiopharmaceutical for myocardial perfusion imaging (Strauss et al. 1975). ^{201}Tl, with a physical half life of 73.1 h, decays by electron capture to ^{201}Hg, which emits useful x-ray photons (69–80 KeV; 94.4% abundance) for gamma camera imaging studies. It is produced in a cyclotron and is indirectly based on the following nuclear reaction.

$$^{203}_{81}\mathrm{Tl}\,(p,3n)\,^{201}_{82}\mathrm{Pb} \xrightarrow{EC,\,9.4\,\mathrm{h}} {}^{201}\mathrm{Tl} \xrightarrow{EC,\,73.1\,\mathrm{h}} {}^{201}_{80}\mathrm{Hg}. \quad (17.1)$$

Following intravenous administration, it is rapidly cleared from the circulation and normal myocardial tissue extracts about 85% of the amount present in the coronary arteries. At pH 4–7, ^{201}Tl predominantly exists as a monocation, and like K^+ ion, it relies on cell-membrane integrity and active metabolic transport using Na^+/K^+ pump for its uptake into the myocardial cells. Approximately 3–5% of the injected dose localizes in the normal myocardial tissue and after initial localization, there is rapid redistribution of ^{201}Tl activity in the myocardium. Early stress-induced defects, which later normalize in redistribution images, imply myocardial ischemia, while persistent defects indicate scarring.

Three important ^{99m}Tc labeled radiopharmaceuticals (Fig. 17.7) were introduced for myocardial perfusion imaging studies (Jain 1999); sestamibi (cardiolite®), tetrofosmin (myoview™), and teboroxime (cardioTec). Six molecules of MIBI (2-methoxy isobutyl isonitrile) bind to the central ^{99m}Tc atom forming a coordination

complex with a single positive charge. As a cationic complex, it is transported into the myocardium by passive diffusion (extraction efficiency < 60%), and the myocardial retention is due to mitochondrial binding. Tetroformin (^{99m}Tc-1,2-bis[bis(2-ethoxyethyl)phosphino] ethane) is also a monocation complex and is transported into the myocardial tissue similar to sestamibi. Teboroxime is a boronic-acid (BATO) derivative and a neutral liophilic compound that passively diffuses into the myocardial cells (extraction efficiency ≈ 90%), but then rapidly washes out. As a result, imaging must be completed with in 10 min following intravenous administration. This compound, however, is not available commercially at this time.

17.3.2 Myocardial Metabolism

Understanding the myocardial metabolism of substrates is very important for understanding the pathophysiology of various cardiac diseases and for designing therapeutic interventions. The heart requires a constant supply of energy to sustain contractile function. The energy is supplied by hydrolysis of ATP, which is primarily derived from the aerobic metabolism. The myocardium chooses between various substrates, such as free fatty acids (FFA), glucose, lactate and ketone bodies (Fig. 17.8) (Bing 1954). The tricarboxylic acid (TCA) cycle is linked to the myocardial oxygen consumption via the electron transport chains, which supply most of the energy in the form of ATP. The amount of oxygen required for oxidation of carbohydrates, glucose or lactate, and fatty acids is summarized in Table 17.4. The selection of an appropriate substrate, however, depends on several conditions, such as plasma concentration of the substrate, hormonal control (insulin, glucagon, and catecholamines levels), stress and physical activity.

In the normal myocardium and also with moderate levels of exercise, FFAs are considered the preferred substrate for metabolism at rest. In the fasting state,

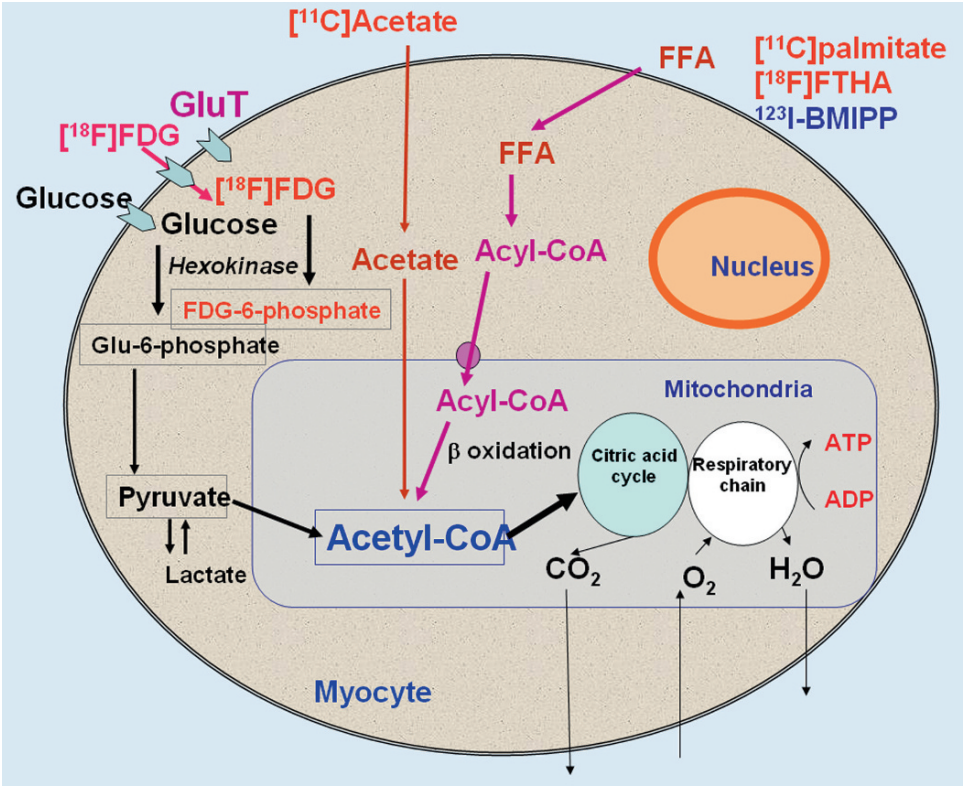

Fig. 17.8 PET and SPECT radiotracers to image myocardial substrate utilization and metabolism

FFA levels in circulation are high and insulin levels are low so that up to 80% of energy is derived from the FFA metabolism. A diet rich in carbohydrates increases the plasma glucose and insulin levels, and then glucose becomes the preferred substrate (Opie and Owen 1975; Heineman and Balaban 1993). With strenuous exercise, the release of lactate into the circulation from skeletal muscle increases and lactate will then become the major fuel for myocardial metabolism.

In various pathological conditions, the myocardial metabolism can be changed significantly. In ischemic myocardium, the oxidative metabolism is reduced and as a result, there is a shift from an aerobic to an anaerobic metabolism. With the lack of a sufficient oxygen supply, glucose is now metabolized to lactate (glycolysis). With ischemia, glucose is the preferred substrate regardless of the availability of other fuels (Opie and Owen 1975; Liedtke 1981). For ischemic heart disease, the major player in the disease pathophysiology is the reduction in regional or focal perfusion. Changes in regional metabolism are a consequence of reduced blood flow to these areas.

Changes in myocardial metabolism may also play a key role in various other cardiac conditions, such as heart failure, cardiomyopathy and diabetes, which involve the myocardium more globally, and involve the myocardium as a whole. However, due to difficulties in evaluating metabolism in human subjects, the alterations in the myocardial metabolism under such conditions are poorly understood Kudo 2007). The substrate utilization may vary depending on the extent of CAD and prior drug therapy to improve LV function. For example, long-term treatment with a β-adrenergic receptor antagonist was reported to be associated with a switch in myocardial metabolism away from FFA oxidation towards glucose metabolism (Wallhaus et al. 2001). Studies in animal models of diabetes mellitus have demonstrated an upregulation of myocardial fatty acid utilization and a reduction of the insulin-mediated glucose transport. However, little is known about the effect of diabetes mellitus on the human heart.

In the near future, the major focus of cardiovascular medicine will move from intervention for acute/chronic coronary disease to primary/secondary prevention. The non-invasive assessment of the metabolism in the ischemic and nonischemic myocardium, based on molecular imaging studies, may play a very important role in understanding the disease development, pathophysiology, and treatment (Kudo 2007; Taki and Matsunari 2007).

17.3.2.1 Glucose Metabolism

Glucose is transported into the myocardial cell by facilitated diffusion of insulin independent, GLUT 1 and insulin dependent, GLUT 4 glucose transporters (Lopaschul and Stanley 1997). Intracellularly, glucose is rapidly phosphorylated to glucose 6-phosphate, which is further metabolized (glycolysis) to pyruvate. Under aerobic conditions, pyruvate is converted to acetyl-CoA, which enters the TCA cycle in the mitochondria for oxidative metabolism (Fig. 17.8). Under anaerobic conditions, pyruvate is further metabolized to lactic acid.

[^{18}F]FDG that enters the myocardium is phosphorylated to FDG-6-phosphate, but then does not enter further metabolic pathways; instead it accumulates in the myocardium. Thus, the myocardial uptake of FDG reflects the uptake and metabolism of glucose (Sokoloff et al. 1977; Phelps et al. 1979). FDG-PET images reflect the relative distribution of FDG uptake in different regions of the myocardium. Also, the metabolic rate (MRglc) of glucose in absolute units can be measured with PET based on dynamic imaging studies, mathematical modeling, compartment model analysis, or graphical plot analysis. Since the rate of the glucose uptake and FDG uptake is not equal, a lumped constant (LC) was developed to convert the FDG uptake to glucose uptake. Usually, the value of LC is fixed, and is approximately 0.6–0.7 for the FDG-PET measurement of MRglc (Krivokapich et al. 1987). The LC, however can vary over a wide range, depending on blood insulin levels and cardiac disease (Botker et al. 1997).

Detection of viability in ischaemic heart disease is one of the most important aspects of the diagnostic and prognostic workup in patients with CAD. In some cases of hibernating myocardium, the resting flow based on PET or SPECT tracers cannot differentiate hibernating myocardium from irreversible myocardial scar formation. Relatively higher FDG uptake in an area of decreased myocardial blood flow in the dysfunctional myocardium, known as “flow metabolism mismatch,” indicates viable myocardium (Tillisch et al. 1986). As a result, FDG-PET is considered as one of the gold standards for the determination of myocardial viability (Fig. 17.9).

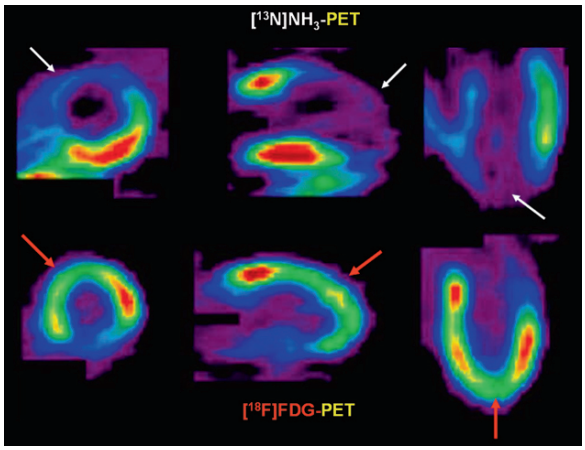

Fig. 17.9 FDG-PET to image myocardial viability. Classic mismatch showing FDG uptake in areas of decreased myocardial perfusion identified by $[^{13}N]NH_3$

17.3.2.2 Fatty Acid Metabolism

Since the FFAs are hydrophobic, they are delivered to the heart by binding to plasma proteins, albumin or lipoproteins. After dissociating from proteins, FFAs easily pass through the myocardial membrane by diffusion or a facilitated transport mechanism. Based on clinical and animal experiments, it has been shown that CD36 plays a crucial role in the fatty acid transport into the cells (Brinkmann et al. 2002; Taki and Matsunari 2007). Intracellularly, FFAs are activated as acylcoenzyme A, (Acyl CoA) and then carried into the mitochondria through an acyl carnitine carrier system and catabolised by β-oxidation into two-carbon fragments, acetyl-CoAs, which enter the TCA cycle for further oxidative metabolism (Fig. 17.8). A part of FFAs is not oxidized but is formed into triglycerides and myocardial structural lipids and stays in the myocardium for a long time. The straight-chain FFAs are generally metabolized through β-oxidation and released from the myocardium, while the development of modified FFAs is based on the concept of myocardial retention from metabolic trapping (Tamaki et al. 2000).

Radiolabeled Fatty Acids for PET

A physiological radiotracer 1-[^{11}C]palmitate (Fig. 17.10) was the first FFA introduced to image fatty acid metabolism of the heart (Schön et al. 1982). Subsequently, 14(*RS*)-[^{18}F]fluoro-6-thia-heptadecanoic acid (FTHA) was developed as a metabolically trapped radiotracer (Stone et al. 1998).

[^{11}C]Palmitate is biologically identical to non-radioactive circulating palmitate. The first pass extraction fraction (0.67) is relatively high and the initial uptake and regional distribution in the myocardium are largely determined by MBF (Schelbert 2004). It clears from the myocardium in a biexponential fashion. Once the tracer is taken up into the myocardium, β-oxidation breaks it down to generate acetyl-CoA. This [^{11}C] acetyl-CoA is oxidised via the citric acid cycle and finally released from the myocardium in the form of $[^{11}C]CO_2$. The rapid clearance fraction corresponds to β-oxidation, whereas the slow-washout fraction reflects the turnover rate of the intracellular lipid pool and is an index of FFA metabolism (Tamaki et al. 2000). In severely ischemic myocardium, the regional uptake of [^{11}C]palmitate is reduced. The PET images provide qualitative and semiquantitative evaluation of fatty acid metabolism. The quantitative value of myocardial fatty acid use and oxidation is difficult to estimate in absolute units (milliequivalents of free fatty acid per minute per gram of myocardium). Since the C-1 label of 1-[^{11}C]palmitate is removed in the initial step of β-oxidation, ω-[^{11}C]palmitate was proposed as a potential tracer to prolong the myocardial retention of trapped metabolites (Buckman et al. 1994).

With FTHA, the rate of metabolic trapping is thought to be proportional to the rate of β-oxidation. In patients with CAD, estimates of myocardial FFA utilization (MFAU) in a normal myocardium was found to be approximately $5.8 \pm 1.7\,\mu mol\ 100\,g^{-1}\ min^{-1}$, while in patients with CHF, the MFAU was found to be elevated ($19.3 \pm 2.3\,\mu mol\ 100\,g^{-1}\ min^{-1}$) (Schelbert 2004; Taylor et al. 2001). Further, because FTHA does not trace the FFA uptake under hypoxic conditions accurately, several ^{18}F analogs have been developed. It is still not clear which tracer is the most reliable or the most clinically useful PET tracer to image fatty acid metabolism in different cardiac diseases (Kudo 2007).

Radiolabeled Fatty Acids for SPECT

Since the 1970s several iodinated fatty acid tracers for SPECT have been developed (Fig. 17.10) by introducing radioiodine to the terminal position of fatty acids without significant alteration of the extraction efficiency,

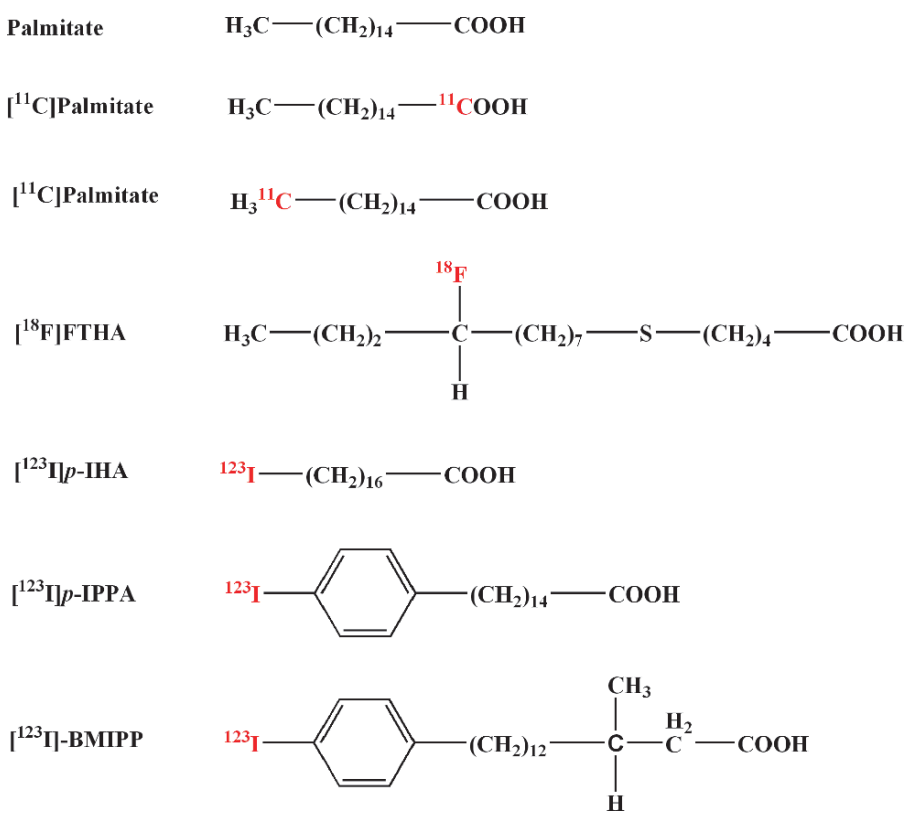

Fig. 17.10 PET and SPECT radiotracers of free fatty acid analogs to assess myocardial metabolism

compared with the natural FFAs (Poe et al. 1977; Tamaki et al. 2000; Taki and Matsunari 2007). The two groups of iodinated fatty acid compounds include straight-chain FFAs and modified branched FFAs. In a clinical study, ^{123}I-17-iodoheptadecanoic acid (IHA), an analog of stearic acid demonstrated a high-quality image early after injection, but the image quality deteriorated rapidly because of the rapid reduction of myocardial counts and increase in background counts due to deiodinated radioiodine (Freundlieb et al. 1980). To prevent in vivo deiodination, the phenyl fatty acids were developed by attaching iodide to the para or ortho position of the phenyl ring (IPPA). For routine clinical use, however, the rate of metabolism and clearance of IPPA is still relatively too fast for SPECT imaging studies.

In order to develop a tracer with more prolonged cardiac retention and with improved image quality, a methyl branching was introduced at the β-carbon position to slow the myocardial clearance by inhibiting β-oxidation. Two iodinated branched fatty acid analogs, 15-(*p*-iodophenyl)-3-R,S-methylpentadecanoic acid (BMIPP) and 15-*p*-iodophenyl)-3,3-methylpentadecanoic acid (DMIPP) were, therefore, developed (Knapp et al. 1986a, b; Tamaki et al. 2000; Taki and Matsunari 2007). FTHA has shown to be metabolically retained in the myocardium and has very good imaging properties in normal human subjects and in patients with CAD. The concept underlying BMIPP imaging is metabolic trapping of BMIPP-CoA, similar to FDG, but by inhibition of β-oxidation through the introduction of methyl branching, at the β-carbon position. Under the condition of ischemia, a reduction in BMIPP uptake is observed, reflecting the reduction in ATP production due to depressed oxidative fatty acid metabolism and substrate shift from fatty acids to glucose (Fig. 17.11). When compared with myocardial perfusion imaging, BMIPP imaging enables "ischemic memory imaging," with detection of previous myocardial ischemia (metabolically stunned myocardium) and viable but chronically dysfunctional myocardium (hibernating myocardium), (Taki and Matsunari 2007). Also, in cardiomyopathy, BMIPP

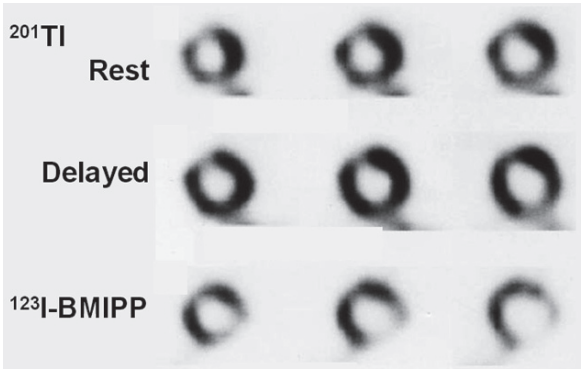

Fig. 17.11 Myocardial metabolic imaging using ^{123}I-BMIPP in patients with unstable angina: Although ^{201}Tl scans did not show definite perfusion abnormalities, decreased BMIPP uptake was noted in the lateral region, indicating decreased regional myocardial metabolism (Tamaki et al. 2000)

Fig. 17.12 Myocardial metabolic imaging using ^{123}I-BMIPP in patients with hypertrophic cardiomyopathy (HCM). There is increased ^{201}Tl uptake in the apex to the anteroseptal wall, but BMIPP uptake is reduced in that area. Discordant BMIPP uptake less than blood flow in the hypertrophic area is a rather early phenomenon of HCM (Taki and Matsunari 2007)

imaging may be useful for the early detection of HCM, the differentiation of ischaemic cardiomyopathy from idiopathic DCM, and also for the prediction of prognosis (Fig. 17.12). ^{123}I-BMIPP has been the most commonly used commercially available SPECT tracer to assess fatty acid metabolism in patients, especially in some of the European countries and in Japan.

17.3.2.3 Oxidative Metabolism

The assessment of myocardial oxidative metabolism involves the estimation of myocardial ventricular oxygen consumption (MVO_2) in absolute units, mL min^{-1} g^{-1}. Under steady-state conditions, MVO_2 provides an accurate measure of overall myocardial metabolism regardless of which substrate or fuel is used. Based on the determination of myocardial blood flow, using [^{15}O] water, myocardial blood volume using [^{15}O]CO, and oxygen inhalation studies using [^{15}O]O_2, myocardial oxygen extraction can be determined. The MVO_2 is then estimated using the plasma oxygen content as the arterial input function. In normal subjects, an average MVO_2 is 0.097 ± 0.022 mL min^{-1} g^{-1} (Yamamoto et al. 1996). While this method provides an absolute quantitative estimation of regional MVO_2 in various cardiac diseases, the PET imaging studies involving ^{15}O ($T_{½}$ = 2 min) are not practical got routine clinical use.

[^{11}C]Acetate

Acetate is avidly extracted from the coronary circulation and rapidly distributed in the myocardium. In cytosol, it is activated to acetyl-CoA and, subsequently, enters the TCA cycle in the mitochondria for oxidation and metabolism to [^{11}C]O_2 and water (Fig. 17.8). It is important to realize that the myocardial kinetics of [^{11}C] acetate is independent of the metabolic milieu, such as the blood glucose level or FFA concentration in the blood (Tamaki et al. 1992). Following intravenous bolus administration, the myocardial wash out of activity demonstrates a biexponential clearance. The myocardial oxidative metabolism, however, can be estimated based on the rapid washout rate determined, using monoexponential curve fitting of the time–activity data (Armbrecht et al. 1989). Because of its high myocardial first-pass extraction fraction, the early phase (1–3 min) is flow dependent and provides an estimation of regional myocardial perfusion (Gropler et al. 1991; Sciacca et al. 2001). With [^{11}C]acetate, simultaneous determination of myocardial blood flow and oxygen consumption can be performed with a single data acquisition (Kudo 2007).

17.3.3 Myocardial Neuronal Imaging

The mammalian heart is characterized by dense adrenergic innervation with a norepinephrine (NE) concentration gradient from the atria to the base of the heart and from the base to the apex of the ventricles. In contrast, parasympathetic innervation is distributed

throughout the atrial and ventricular walls, with a gradient from the former to the latter, with acetylcholine (ACh) being the main neurotransmitter. Both, the sympathetic and parasympathetic tone control the rate of the physiologic stimulation and conduction, while the contractile performance is primarily modulated by sympathetic neurotransmission. The major neurotransmitters of the sympathetic and parasympathetic systems, NE and ACh, define the stimulatory and inhibitory physiologic effects of each system.

The NE is produced from tyrosine within a neuron (Fig. 17.13). Tyrosine is converted to DOPA, which is converted to dopamine by *DOPA decarboxylase*. Dopamine is then transported by a vesicular monoamine transporter (VMAT2) into the vesicles, where it is converted to NE by dopamine β-hydroxylase. Adrenergic nerve stimulation leads to the release of NE into the synapse. The sympathetic neurotransmission in the heart is mediated by adrenoreceptors of type β_1 and β_2, which are located on the myocardial cells. Only a small amount of NE, released into the synapse, binds to the adrenoreceptors while most of the NE in the synapse undergoes reuptake (uptake-1 mechanism) back into the presynaptic nerve terminal by a saturable and Na^+, temperature, and energy dependent mechanism (uptake-1) via a neuronal norepinephrine transporter (NET) or by nonsaturable, and not Na^+, temperature or energy dependent mechanism (uptake-2). The free cytosolic NE is degraded by MAO to dihydroxyphenylglycol (DHPG).

Choline, the precursor for the synthesis of ACh is transported into the parasympathetic presynaptic nerve terminal, where *choline acetyl transferase* (ChAT) catalyses the reaction between acetyl CoA and choline. ACh is then stored in the vesicles and upon nerve stimulation is released into the cholinergic synapse where it binds to specific receptors (mAChR). Within the synapse, ACh is also rapidly degraded by *acetylcholinesterase* (AChE) acetate and choline.

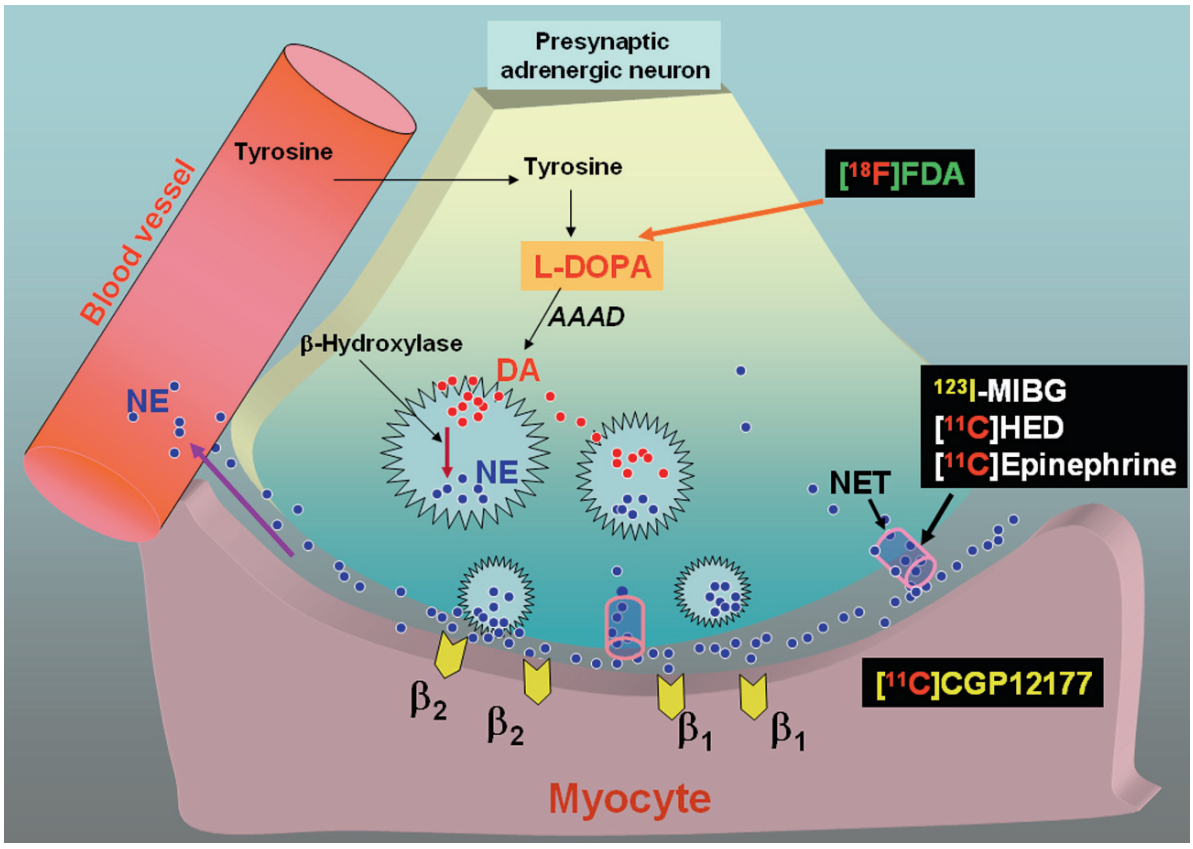

Fig. 17.13 Adrenergic neurotransmission in the heart. PET and SPECT tracers for imaging presynaptic adrenergic neurons and postsynaptic adrenoceptor density

With conventional anatomic imaging techniques, it is not possible to separate nerve fibers from myocardial or vascular cells. Using molecular imaging radiotracers, that are specifically retained in the neuronal structures, it is possible to image the cardiac neuronal innervation and regional distribution.

17.3.3.1 Radiotracers for Presynaptic Sympathetic Innervation

All of the radiotracers developed for imaging cardiac sympathetic innervation are analogs of NE (Fig. 17.14). As discussed earlier, NE within the synapse is transported back into the presynaptic neuron terminals via NETs, based on the uptake-1 mechanism. Structural analogs of NE such as epinephrine, guanethidine, and metaraminol are also transported into synaptic terminals by this uptake-1 mechanism (Raffel and Wieland 2001)

^{123}I-MIBG

Guanethidine is a potent neuron-blocking agent that acts selectively on sympathetic nerve endings. Based on this molecule, ^{131}I-*meta*-iodobenzylguanidine (MIBG) was initially developed as an agent for imaging

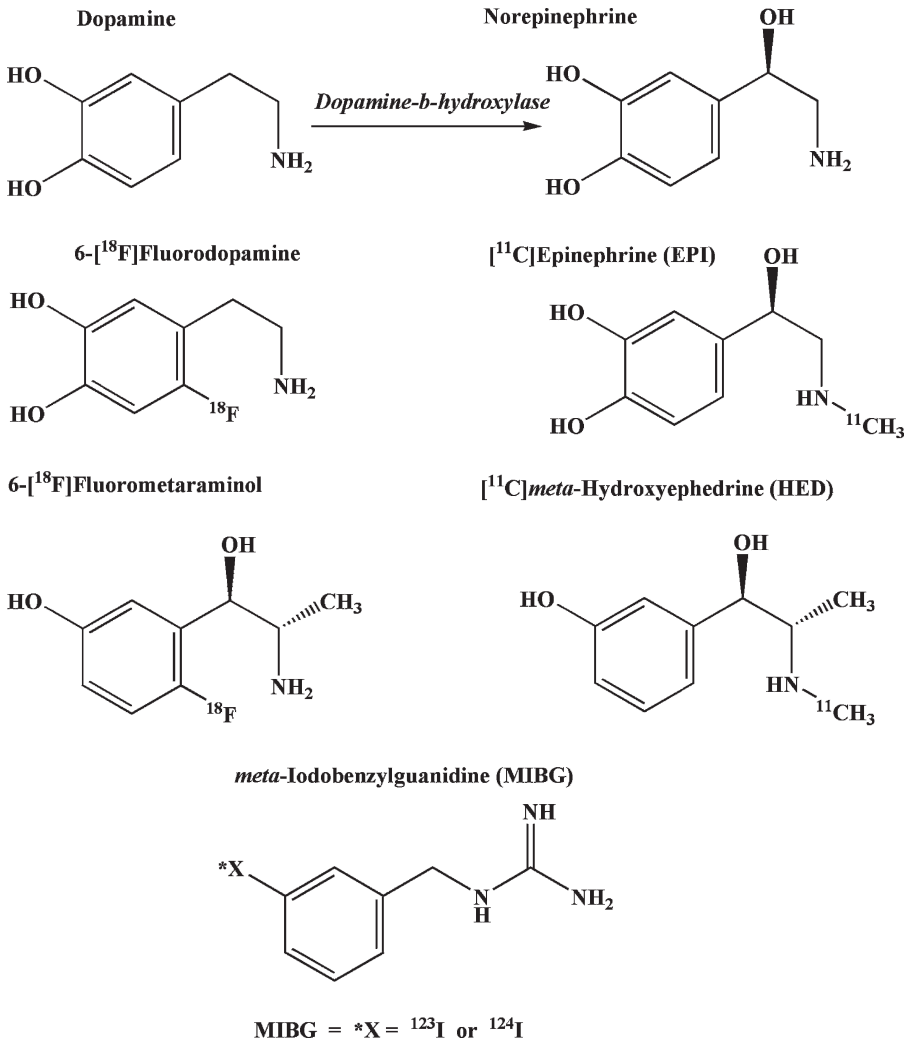

Fig. 17.14 Norepinephrine analogs labeled for PET and SPECT imaging studies to assess cardiac neurotransmission

tumors of adrenal medulla origin (Wieland et al. 1979). The avid heart uptake and retention of MIBG observed in animal biodistribution studies strongly suggested that MIBG might also be successfully used for imaging cardiac sympathetic neurons (Wieland et al. 1981). Consequently, ^{123}I-MIBG was developed for imaging the heart, in patient studies (Kline et al. 2001). MIBG is transported into presynaptic terminals by the uptake-1 mechanism and is stored mainly in the NE storage vesicles. In other words, MIBG and NE have the same mechanisms for uptake, storage and release. Unlike NE, MIBG does not bind to receptors on the myocardial cell membrane, and does not undergo any metabolism within the presynaptic terminals (Carrió 2001; Yamashina and Yamazaki 2007). As a result, MIBG is retained in sympathetic nerve endings, and provides clinically useful diagnostic information for different cardiac diseases.

For practical clinical application the SA and radiochemical purity of MIBG are critical factors. The unlabeled catecholamines (cold MIBG) may compete with the labeled tracer and may not only limit image quality but also cause pharmacologic action via adrenoceptor activation. Therefore, high SA ^{123}I-MIBG (1,665–2,035 MBq mg^{-1}) may be beneficial for clinical studies.

Radiotracers for PET

PET radiotracers (Fig. 17.14) resemble the endogenous NE more closely than MIBG. Two different groups of PET tracers are available for presynaptic sympathetic imaging of the heart; radiolabeled catecholamines and radiolabeled catecholamine analogs (Carrió 2001; Lautamäki et al. 2007).

[^{11}C]Hydroxyephedrine (HED) is the most widely used tracer for cardiac neuronal imaging. HED has high affinity for the NETs and shows negligible nonspecific binding. Following transport into the presynaptic terminal, it is not metabolized by *MAO* or *COMT* enzymes (Rosenpire et al. 1990; Carrió 2001). Since HED is not metabolized, it diffuses out of the nerve terminal and is transported back into the nerve terminal. Therefore, HED myocardial retention is actually dependent on both the continuous release and reuptake by NETs (Lautamäki et al. 2007).

While HED is a false neurotransmitter, [^{11}C]epinephrine (EPI) is a more physiological tracer since it is primarily a circulating hormone produced together with NE by the adrenal medulla and other chromaffin tissues. Unlike HED, EPI is degraded by MAO, but its storage in the vesicles is very efficient, preventing it from degradation and causing slow clearance of the tracer from the heart. Therefore, EPI reflects the whole cascade of uptake, metabolism, and storage of neurotransmission, while the primary target for HED and MIBG is the uptake-1 system. Both, HED and EPI can be synthesized with high chemical purity (> 95%) and SA (33–74 GBq μmol^{-1}). As a result, ^{11}C tracers may be better compared to the MIBG preparation for quantitative measurement of presynaptic NETs in cardiac disease.

6-[^{18}F]fluorodopamine has been safely used in humans to assess cardiac and extracardiac sympathetic innervation. Based on the synthesis method used, one can obtain SA in the range of 7,400–29,600 MBq mmol^{-1} (Carrió 2001). Following intravenous administration, it is transported into the presynaptic sympathetic nerve terminals via the uptake-1 mechanism, after which it is rapidly internalized into the vesicles and β-hydroxylated, forming radiolabeled NE (Goldstein et al. 1993). The release of this tracer into the synapse and reuptake into the nerve terminal are similar to NE. However, [^{18}F]fluorodopamine, can undergo extensive metabolism in vivo. While this tracer is potentially useful to assess NE synthesis, transport and storage in the vesicles of presynaptic adrenergic neurons, PET quantitation needs the incorporation of the fluorodopamine metabolism in the compartmental modeling techniques.

17.3.3.2 Radiotracers for Cardiac Neuroreceptors

The sympathetic adrenoreceptors β_1 and β_2, located on the myocardial cells, play a major role in the regulation of cardiac function. In the healthy myocardium, β_1-receptors are the most abundant, forming 80% of all β-receptors, while in heart failure the proportion of β_2-adrenoceptors may increase to 50% (Schaèfers et al. 2002; Lautamäki et al. 2007). Also, sympathetic activation results in the elevation of systemic catecholamine levels and subsequent down regulation of β-receptors. Many different pharmaceuticals, that act as cardiac receptor antagonists, such as β-blockers or β-receptor antagonists, are used in cardiological practice. The efficacy of these drugs depends on many different factors, especially the β-receptor density. Noninvasive imaging and quantitation of β-receptor

density (B_{max}) before initiation of therapy with β-blockers might predict the outcome of therapy.

[^{11}C]CGP-12177 (4-(3-*t*-butylamino-2-hydroxypropoxy) -benzimidazol-1), a hydrophilic, nonselective antagonist (Fig. 17.8), that binds to the β-receptors with high affinity (0.3 nmol L^{-1}), was one of the first ligands developed for cardiac PET adrenoreceptor imaging studies (Delforge et al. 1991). CGP-12177 can be labeled with ^{11}C using CGP-17704 and ^{11}C-phosgene as precursors. Subsequently, a number of β-blockers, such as pindolol, atenolol, propranolol, carazolol, metoprolol have all been labeled with ^{11}C, but none of these agents have optimal imaging characteristics. So far, [^{11}C]CGP-12177, is the only tracer, that has been used more extensively in patient populations, such as patients with dilated hypertrophic and arrhythmogenic right ventricular cardiomyopathy (Carrió 2001; Lautamäki et al. 2007). Because of the difficulties involved in the synthesis of this tracer, the *N*-isopropyl derivative, [^{11}C]CGP-12388 was developed as an alternative for clinical use (Elsinga et al. 2004).

Carazolol is a lipophilic, nonselective β-adrenoceptor antagonist and can be labeled with either ^{11}C or ^{18}F (Berridge et al. 1994). The in vivo binding is stereoselective because the *R*-isomer does not accumulate in the target organs.

17.3.3.3 Clinical Applications

Clinical PET findings in diseases associated with cardiac neuronal dysfunction of the adrenergic system are summarized in Table 17.3. MIBG myocardial scintigraphy is one of the few methods available for objectively evaluating cardiac sympathetic function at the clinical level, and provides an abundance of information useful for the evaluation of various heart diseases (Yamashina and Yamazaki 2007). Sympathetic nerve endings are easily damaged by ischemia, in comparison to myocardial cells, and sympathetic function disorders are known to persist for a certain period even after alleviation of the ischemia. In patients with unstable angina, MIBG-SPECT makes it possible to identify the culprit coronary artery with a high probability, and, thus is of diagnostic value (Fig. 17.15). In patients with heart failure, the increased washout rate and the decreased heart/myocardium (H/M ratio) on the delayed MIBG image become marked with an increase in hypofunction in the left ventricle, regardless of the underlying diseases (Imamura et al. 1995). Similar results have been reported from studies on dilated cardiomyopathy, hypertrophic cardiomyopathy (HCM), valvular heart disease, pulmonary hypertension, amyloidosis and diabetes (Yamashina and Yamazaki 2007).

Table 17.3 PET and SPECT studies to assess myocardial neuronal transmission

Disease	Radiotracer	Findings
Heart failure	[^{11}C]HED	Globally and regionally decreased uptake
	[^{11}C]CGP12177	Reduction in β-adrenoceptor density
	[^{11}C]CGP12388	
	^{123}I-MIBG	Increased washout rate and the decreased heart/myocardium ratio on the delayed MIBG image become marked with an increase in hypofunction in the left ventricle
Heart transplant	[^{11}C]HED	Denervated hearts show no tracer uptake.
Diabetes	[^{11}C]HED	Tracer uptake reduced in neuropathy. Sympathetic dysinnervation is related to impaired coronary reserve and diastolic dysfunction
CAD	[^{11}C]HED	Sympathetic dysinnervation in chronic CAD
	[^{18}F]Fluorodopamine	Association between coronary reserve and segmental tracer uptake
	^{123}I-MIBG	Decreased regional myocardial uptake in patients with unstable angina and vasospastic angina, and in nonQ-wave myocardial infarction
	[^{11}C]CGP12177	Reduced β-adrenoceptor density after myocardial infarction
Arrhythmias	HED	Normal, increased or reduced uptake
	[^{11}C]CGP12177	Decreased β-adrenoceptor density in patients with arrhythmogenic right ventricular cardiomyopathy and in RVOT tachycardia

Note: The above table was modified from Lautamäki et al. (2007)

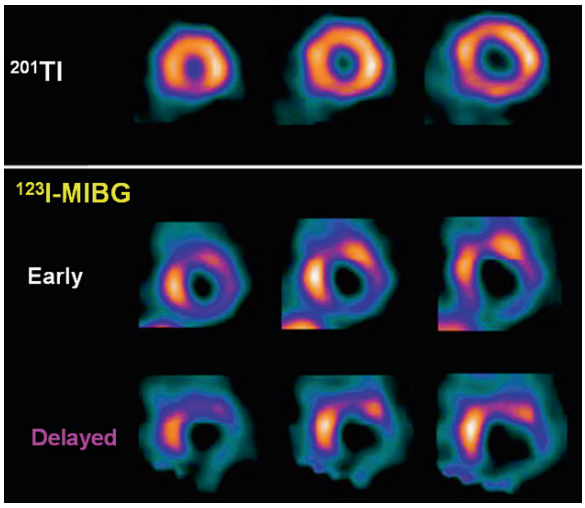

Fig. 17.15 ^{123}I-MIBG imaging in patient with ischaemic heart disease. In a patient with unstable angina, myocardial perfusion with ^{201}Tl-SPECT at rest was relatively normal with no significant findings. In contrast, MIBG SPECT (early and delayed) showed decreased accumulation in the infero-posterior wall. Coronary angiography performed later, advanced stenosis was recognized in the proximal part of the RCA (Yamashina and Yamazaki 2007)

PET imaging of the cardiac autonomic nervous system has advanced extensively in recent years, and multiple pre- and postsynaptic tracers have been used to determine the involvement of the sympathetic dysinnervation at different stages of heart diseases, such as ischemia, heart failure, and arrhythmia. In general, [^{11}C]HED is the most widely used PET tracer for cardiac neuronal imaging. In a healthy heart, there is an even distribution of HED over the left ventricle, making it a valuable tracer for detecting specific regional defects of the presynaptic sympathetic system in disease (Lautamäki et al. 2007). In patients with dilated cardiomyopathy there is a loss of neurons or downregulation of uptake-1. In a patient with idiopathic dilated cardiomyopathy and severely reduced left ventricular ejection, the myocardial retention of HED was reduced significantly (Fig. 17.16). Similarly, a PET study with [^{11}C]-CGP12177 has shown that in patients with idiopathic dilated cardiomyopathy, there is a significant reduction in the amount of left ventricular β-adrenoceptors (Merlet et al. 1993).

17.3.4 Angiogenesis

Angiogenesis is a process fundamental to neovascularisation stimulated by inflammation and ischemia. Angiogenesis is generally defined as the growth and development of new capillary blood vessels from

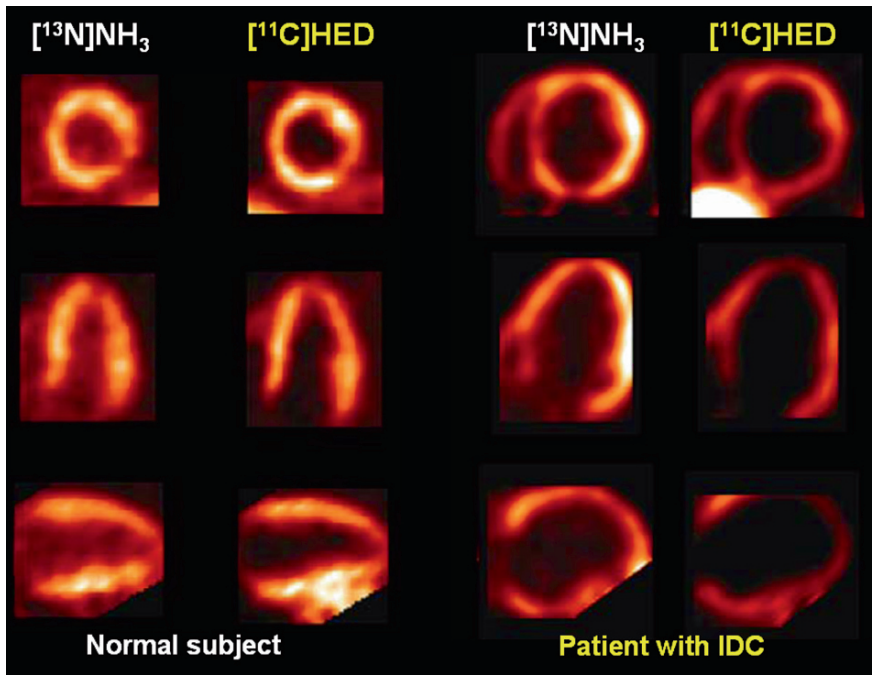

Fig. 17.16 [^{11}C]HED-PET for imaging presynaptic sympathetic innervation in the heart. In a normal subject, there is an even distribution of HED in the heart similar to the myocardial perfusion images of [^{13}N] ammonia-PET. In a patient with idiopathic dilated cardiomyopathy (IDC) and severely reduced left ventricular ejection fraction (22%), there is a significantly reduced retention of HED compared with the myocardial perfusion (Lautamaki et al 2007)

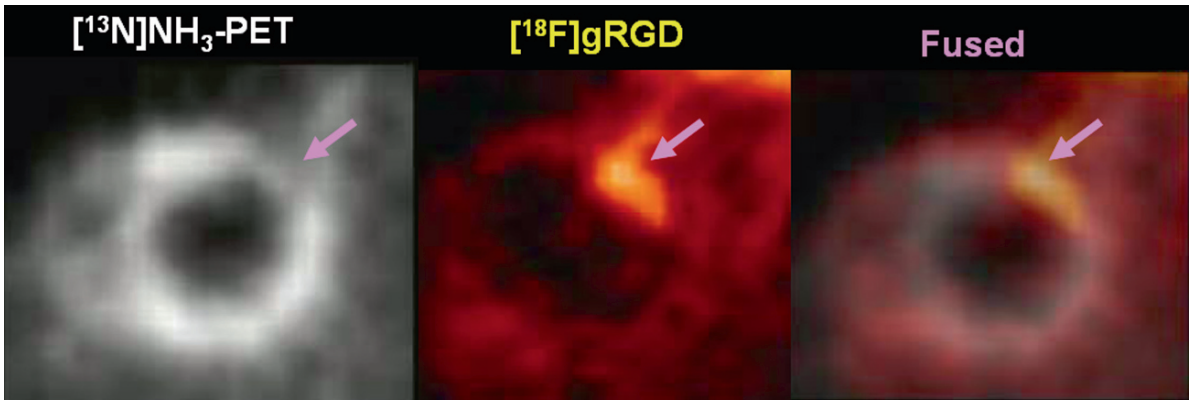

Fig. 17.17 ^{18}F-galacto-RGD, a specific radiotracer to image angiogenesis based on αvβ3 integrin expression in a rat model of coronary occlusion. In vivo short axis MicroPET images demonstrate a focal uptake of galacto-RGD in an area with a decrease in myocardial perfusion. The images were obtained 1 week after the ischaemic event (Higuchi et al 2007)

preexisting vasculature involving mature endothelial cells (Carmeliet 2000). Myocardial ischemia causes reversible or irreversible myocardial injury and triggers the formation of collateral vessels via angiogenesis, which occurs as part of the natural healing process after ischemic injury. The process of angiogenesis involves a complex interplay of many molecules and cells (vascular smooth muscle cells, endothelial cells, macrophages, and circulating stem cells), as well as the extracellular matrix (ECM) (Higuchi et al. 2007). Migration and proliferation of endothelial cells are promoted by angiogenic factors, such as vascular endothelial growth factor (VEGF) and basic fibroblast growth factor (bFGF), which are released from the endothelial and inflammatory cells via transcription factors, such as activation of hypoxia-inducible factors (HIFs). During angiogenesis endothelial cells must adhere to one another and to the ECM to construct and extend new microvessels. Integrins, a family of heterodimeric cell surface receptors capable of mediating cell adhesion, migration, proliferation, differentiation, and survival play a major role in the angiogenic response. Among them, $\alpha_v\beta_3$ integrin has been identified as a critical modulator of angiogenesis. Radiolabeled tracers targeting αvβ3 integrin expression was evaluated in animal models of myocardial ischemia using ^{18}F-galacto-RGD, ^{111}In-RP747, and ^{99m}Tc-NC100692 (Higuchi et al. 2007). In preclinical studies, ^{18}F-galacto-RGD has shown focal tracer accumulation in the ischaemic heart in specific areas that have decreased perfusion on [^{13}N]ammonia-PET, one week after the ischaemic event (Fig. 17.17). Further, the in vivo image data showed excellent correlation with autoradiographic data.

VEGF is one of the most important and potent angiogenic factor in the regulation of endothelial cell proliferation. Expression of the VEGF gene and VEGF receptors is strongly enhanced by hypoxia in the angiogenic process. Therefore, VEGF receptors are good candidates for imaging angiogenesis in ischaemic tissues. ^{111}In-labeled recombinant human $VEGF_{121}$ has shown specific tracer localization in a rabbit model of unilateral hindlimb ischemia (Lu et al. 2003).

Matrix metalloproteinases (MMP) are proteolytic enzymes that cause extracellular protein degradation and are involved in the endothelial cell migration and growth factor liberation. MMPs are also responsible for the left ventricular remodeling by degrading extracellular matrix in the heart after myocardial infarction. Recently, Su et al. demonstrated the feasibility of MMP activation imaging in a murine model of myocardial infarction. Further ^{111}In and ^{99m}Tc labeled RP782 were developed and evaluated in animal models (Su et al 2005).

17.3.5 Vulnerable Plaque and Atherothrombosis

The executive summary of the screening for heart attack prevention and education (SHAPE) task force report, published in 2006, suggests that a molecular imaging technique that could accurately identify the site of vulnerable plaques should be one of the four

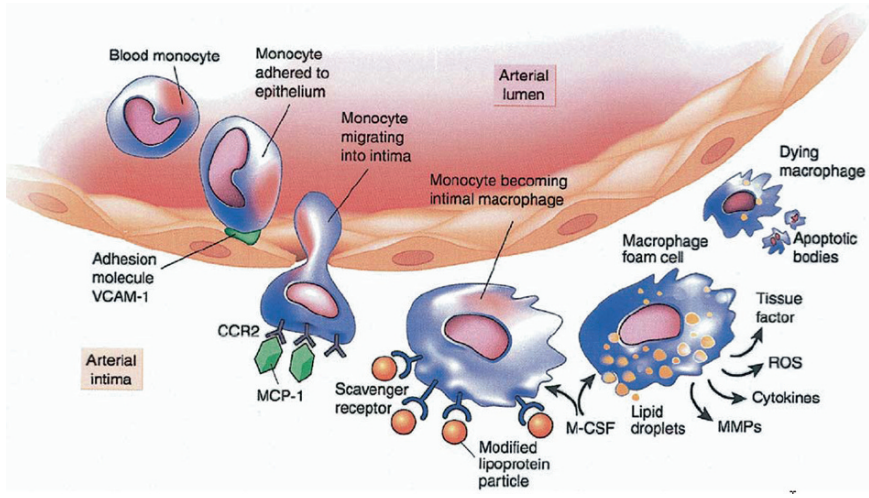

Fig. 17.18 The biology of atherosclerosis initiation, progression, and complications. CCR2 = chemokine (CC motif) receptor 2; MCP = monocyte chemoattractant protein; M-CSF = monocyte colony-stimulating factor; MMP = matrix metalloproteinase; ROS = reactive oxygen species; VCAM = vascular cell adhesion molecule. (From Jaffer et al 2006)

major areas of future research in CAD (Naghavi et al. 2006). A number of noninvasive and invasive diagnostic imaging techniques are being evaluated to accurately identify high-risk individuals, based on the presence of high-risk anatomical or structural features of atherosclerotic plaques in the coronary arteries. However, imaging coronary lesions is a challenge since they are contained within the wall of the vessel, and typically these lesions occupy a fraction of the vessel circumference and often extend from 1 to 2 cm. In addition, the residual activity of the radiotracer in blood, and the myocardial tissue uptake of the radiotracer make these lesions more difficult to detect. Molecular imaging technique based on specific β^+ emitting radiotracers, however, may provide the potential to detect coronary atherosclerotic lesions.

The biology of atherosclerosis (Fig. 17.18) provides a basis for the development of radiolabeled molecular imaging probes. Fundamentally, the process of inflammation regulates atherosclerosis. Specifically, the macrophage has emerged as the key cellular mediator of inflammation in atheroma, and participates in all phases of atherogenesis, including lesion initiation, progression, and complication (Falk 2006; Jaffer et al. 2006). Following the initial recruitment of monocytes into the arterial wall, the cells mature into macrophage, which ingest oxidized lipoproteins, become foam cells, and, thus, contribute to the atheroma expansion. A subset of macrophages can die within the atheroma, via oncosis and/or apoptosis (programmed cell death), leading to the development of a paucicellular lipid core. Macrophages also produce and/or secrete a number of proteases, such as cathepsins and matrix metalloproteinases (MMP), that can degrade the extracellular matrix comprising the fibrous cap. Autopsy studies have demonstrated prominent macrophage accumulation in ruptured atherosclerotic lesions (Davies et al. 2006). These findings underscore the key role of macrophages in plaque complications (Naghavi et al. 2006). Under inflammatory conditions, endothelial cells express adhesion molecules, such as VCAM-1. In addition, the fragile endothelium in angiogenic vessels, typically associated with $\alpha_v\beta_3$ integrin, can promote lesion progression via intraplaque hemorrhage and may produce plaque complications. Apoptosis of both macrophages and vascular smooth muscle cells is seen in the wall of atherosclerotic vessels. Smooth muscle cells undergoing programmed death in the fibrous parts of plaque have been shown to express genes encoding for inflammatory cytokines and chemoattractant factors (Libby 2002), and colocalize with oxidized low-density lipoprotein. Apoptosis of macrophages is found in the vulnerable plaque. Thus, the biology of atherosclerotic lesion itself provides the basis for the development of atherosclerosis-targeted molecular imaging probes (Table 17.4). In order to identify the most specific radiotracers for imaging vulnerable plaques in patients who are at very high risk, several promising imaging agents need comparative evaluation in the same animal model, under similar pathophysiological conditions.

Table 17.4 Atherothrombosis: Imaging targets and radiotracers

Biological process	Class	Specific molecular target	Radiotracer
Cholestrol transport	Lipid core	Low density lipoprotein (LDL)	^{99m}Tc or ^{111}In-LDL Radiolabeled peptides (based on Apo B-100)
Macrophage activity	Surface receptors	Scavenger receptor A, Monocyte chemoattractant peptide (MCP)	^{99m}Tc-oxidized-LDL
		Peripheral Benzodiazepine receptor	^{123}I-MCP-1
			^{123}I- or [^{11}C]PK11195
	Metabolism	*Hexokinase Choline kinase*	[^{18}F]FDG, [^{18}F]Fluorocholine
	Proteases	Matrix metalloproteinase (MMP),Cathepsins	^{123}I-HO-CGS 27023A (MMP inhibitor)
	Peroxidases	Myeloperoxidase (MPO)	[methyl^{11}C]ABAH
	Modified lipoproteins	Oxidized LDL,	^{99m}Tc-oxidized-LDL
Angiogenesis	Increased vascularity	Perfusion markers	
	Endothelium	VCAM-1, E-selectin $\alpha_v\beta_3$ integrin	^{64}Cu-DOTA-RGD
			^{18}F-gluco-RGD
			^{111}In-RP748
			^{111}In-VEGF121
Apoptosis	Cell membrane	Phosphatidylserine	^{99m}Tc-Annexin V (A5)
			^{18}F-annexin V
			^{64}Cu-DOTA-Annexin V
	Enzymes	Caspases, scramblases	
Cell trafficking	Monocytes, lymphocytes, Stem cells	Specific molecular target	Radiolabeled cells
Thrombosis	Activated platelets	GP IIB/IIIA RGD peptides	^{111}In or ^{64}Cu-DOTA-P280, P748 peptides

Radiotracer	E	MBF (mL min^{-1} g^{-1})	
		Rest	Stress[a]
[^{15}O]Water	0.96 ± 0.05	0.90 ± 0.22	3.55 ± 1.15
[^{13}N]Ammonia	0.83–0.60	*Glutamine synthase*	
^{82}Rb chloride	0.68–0.60	0.80 ± 0.26	
^{62}Cu-PTSM			

[a]After intravenous dipyridamole

17.3.5.1 Radiotracers for Vulnerable Plaque

In the 1970s it was first demonstrated that ^{125}I-labeled LDL localizes in the carotid atherosclerotic lesions in human subjects (Lees et al. 1983). Since that time a number of radiolabeled LDL preparations, antibodies, and peptides have been extensively evaluated in animal models as potential radiotracers for imaging atherosclerotic lesions (Vallabhajosula et al. 1995).

Molecular imaging based on PET and SPECT radiotracers is a rapidly evolving discipline that aims to develop imaging agents and technologies to visualize the specific molecular processes associated with vulnerable plaque. In the 1990s, it was demonstrated that FDG-PET identifies macrophage rich atherosclerotic lesions in hypercholesterolemic rabbits (Fig. 17.18) (Vallabhajosula et al. 1995; Vallabhajosula and Fuster 1997). It was also shown that FDG-PET is useful to detect the atherosclerotic lesions in the carotid arteries of patients undergoing surgery (Fig. 17.19) (Rudd et al. 2002). Based on the carotid specimens from these patients, it was also shown that FDG specifically localizes in the macrophages very close to the fibrous cap. Subsequently, localization of FDG in human atheromas has been documented for the carotid arteries, aorta and other major vessel (Weissberg 2004; Ben-Haim and Israel 2006). The potential of FDG-PET to identify vulnerable plaques characteristic of subclinical coronary disease, however, has not yet been validated. Several other radiotracers have also been proposed as specific markers for imaging vulnerable plaque and atherosclerosis (Table 17.4).

(*R*)-[11C]PK11195 (1-[2-chlorophenyl]-*N*-methyl-*N*-[1-methyl-propyl]-3-isoquinoline carboxamide) is a

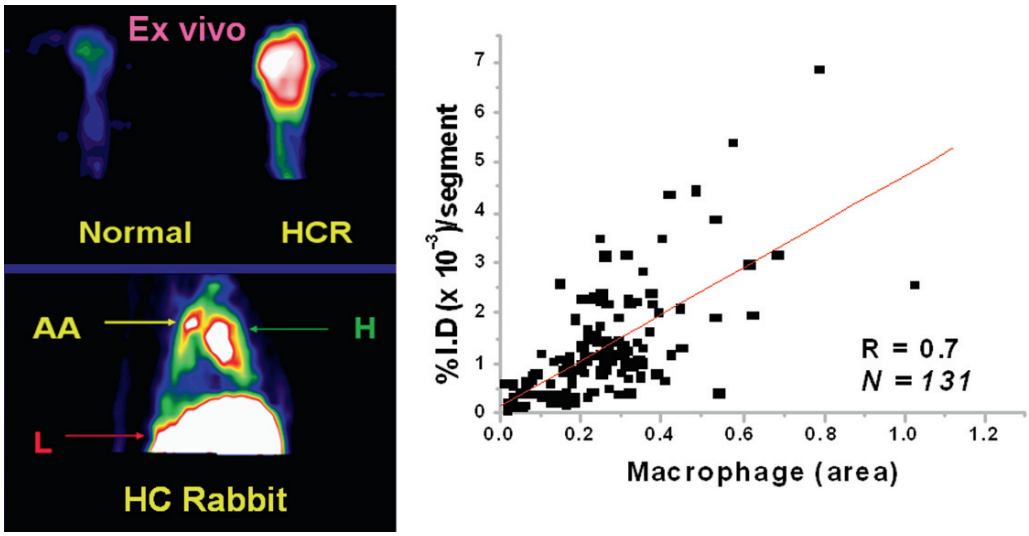

Fig. 17.19 [^{18}F]FDG-PET to image atherosclerosis in hypercholeterolemic rabbits (HCR). The bottom in vivo image shows FDG uptake in the ascending aorta (AA) of HCR while the top ex vivo image shows comparison of HCR and normal aortas. The FDG uptake in the atherosclerotic lesions appears to depend on the macrophage density

specific ligand for the peripheral benzodiazepine binding site, which is particularly abundant on cells of the mononuclear phagocyte lineage. Several investigators have previously used this tracer to image activated microglia/brain macrophages (Banati 2003). Choline is taken up into cells and phosphorylated by choline kinase, metabolized to phosphatidylcholine, and eventually incorporated into the cell membrane. [^{18}F]fluorocholine (FCH) has been introduced as a tracer for tumor, but it also is taken up by macrophages. Recently, FCH has been shown to be taken up by murine atherosclerotic lesions ex vivo and the uptake of FCH was even greater than that of FDG (Matter et al. 2006). As discussed above, apoptosis is a potential target for imaging atherosclerosis since annexin V specifically binds to apoptotic cells with nanomolar affinity. ^{99m}Tc-Annexin V has shown strong uptake in the balloon injured aortas of cholesterol-fed rabbits and identified coronary atherosclerotic lesions in a porcine model of atherosclerosis. In a clinical study, ^{99m}Tc-Annexin V has demonstrated in vivo uptake into carotid plaques, containing macrophages and intraplaque hemorrhage, but not in the carotid plaques with stable histological features (Kietselaer et al. 2004). Annexin V has been labeled with other SPECT radionuclides (^{123}I and ^{111}In) and can be also be labeled with PET radionuclides, such as ^{18}F, ^{124}I and ^{64}Cu. Matrix metalloproteases (MMP) can degrade extracellular matrix macromolecules, including elastin and collagen. Further, increased MMP activity in humans suggests a causative role for MMPs. Imaging of MMP activity in atherosclerosis, therefore, offers another method for detecting inflamed atherosclerotic lesions.^{123}I and ^{111}In labeled compounds that bind to MMP were recently shown to be taken up by carotid lesions in a mouse model (Schafers et al. 2004). Myeloperoxidase (MPO) is also present within human atherosclerotic plaques and its products may promote atherogenesis by modifying LDL to an atherogenic form, functionally inactivating HDL, activating MMPs, causing endothelial cell apoptosis, tissue factor release, and inactivation of nitric oxide. Recently benzoic acid hydrazides have also been identified as preferred inhibitors of MPO. Among these agents, 4-aminobenzoic acid hydrazide (ABAH) is the most potent inhibitor identified to date. Its binding leads to irreversible inactivation of the enzyme by a suicide substrate mechanism.

The "high risk," "thrombosis prone," and "vulnerable" plaques all describe a plaque that is at increased risk of thrombosis and rapid stenosis progression. Since these plaques are often not identified, before causing clinical events, there is great need to identify these plaques before the onset of symptoms. Based on noninvasive imaging techniques, patients identified as being at "high-risk" need further stratification to identify those with vulnerable plaques who are at "very high

risk." The development of novel imaging modalities capable of detecting vulnerable plaques is hindered by the lack of a suitable animal model with plaque characteristics that have clinical relevance. Also, the design of radiotracers capable of detecting and characterizing rupture-prone lesions in humans, may eventually lead to the development of (a) noninvasive, relatively safe, screening technique to identify patients with subclinical disease and (b) innovative therapeutic alternatives designed to "passivate" the plaque with the potential of preventing future major cardiovascular events.

17.3.5.2 Radiotracers for Intraarterial Thrombus

Blood clots or thrombi in veins are generally composed of layers of zones of polymerized fibrin with entrapped plasma proteins and red cells (red thrombus), interspersed with whitish layers primarily composed of aggregated platelets. In arteries and in areas where the thrombus is exposed to high blood flow rates, the thrombus may predominantly consist of activated platelet aggregates. In contrast, when the thrombus is completely occlusive, where the blood flow is sluggish, the thrombus may predominantly consist of fibrin deposits. In order to develop molecular imaging probes to image thrombus in vivo, radiotracers have been developed based on two different approaches; Radiotracers that bind specifically to fibrin or to activated platelets. Radioiodinated (^{125}I or ^{123}I) fibrinogen was introduced almost three decades ago for imaging deep vein thrombosis (DVT). Subsequently, platelets labeled with ^{111}In oxine were introduced for imaging active thrombi in vivo. Since radiolabeled fibrinogen and platelets have long circulation times a number of radiolabeled peptides and polypeptides have been developed for thrombus imaging. The development of radiopharmaceuticals for thrombus detection have been reviewed extensively (Knight 2001; Taillefer 2001)

Autologous platelets can be labeled efficiently with ^{111}In or ^{99m}Tc- lipophillic complexes, such as oxine and tropolone. A number of clinical studies have demonstrated ^{111}In-platelet uptake in atherosclerotic lesions of carotid and femoral arteries, and in the abdominal aorta (Knight 1990, 2001).The $\alpha_{IIb}\beta_3$ integrin (GP IIb/IIIa receptor) on platelets is the most commonly targeted receptor for imaging platelet deposits in thrombi. These receptors are present in high concentrations on activated platelets with fibrinogen being main ligand for these receptors. The main binding region of fibrinogen contains a tripeptide motif RGD (Ag–Gly–Asp). Further, it has been shown that a number of small peptides containing RGD sequence also bind to these receptors. It has also been observed that in addition to the RGD sequence other tripeptide motifs, such as RYD (Arg–Tyr–Asp) present in PAC-1 antibody and KGD present in polypeptides known as disintegrans (such as bitistatin), bind to the glycoprotein IIb/IIIa receptor on activated platelets. A number of linear peptides (such as PAC-3 and PAC-8) and cyclic peptides (such as DMP-728, MK-0852 and integrilin) containing RGD or RYD motifs were developed. Among the cyclic peptides, integrilin is an FDA approved antithrombotic drug, while ^{99m}Tc-P280 or Apcitide (AcuTect) is approved for imaging DVT (Taillefer 2001; Knight 2003).

Radioiodinated fibrinogen was the first scintigraphic agent used successfully to detect thrombus. This tracer localizes only in actively growing thrombus, but requires delayed imaging for optimal diagnostic accuracy because the plasma clearance of the tracer is very slow. Fibrinogen is a bivalent plasma protein consisting of three polypeptide chains (a, b, and g). During clotting, the enzyme, thrombin cleaves the fibrinopeptides from the fibrinogen leading to the formation of a fibrin polymer. Within hours after acute thrombus formation, a number of fibrin degradation products are formed. Both, 1^{23}I and ^{99m}Tc labeled fibrin fragment E1 (60 kDa) have shown excellent thrombus uptake in vivo (Knight 1993). In addition it has been shown that a peptide with the sequence, Gly–Pro–Arg–Pro, is capable of inhibiting fibrin polymerization. It has also been shown that the pentapeptide, Gly–Pro–Arg–Pro–Pro (GPRPP), has the highest fibrinogen/thrombin clotinhibiting activity (Laudano and Doolittle 1978). An analog of GPRPP, ^{99m}Tc-TP850 with high affinity for a chain of fibrin polymer was also found to localize, in a swine model of experimental deep venous thrombosis and pulmonary emboli (Thakur et al. 2000; Aruva et al. 2006).

References

Arimoto T, Takeishi Y, Fukui A, et al (2004) Dynamic ^{123}I-MIBG SPECT reflects sympathetic nervous integrity and predicts clinical outcome in patients with chronic heart failure. Ann Nucl Med 18:145–150

Armbrecht JJ, Buxton DB, Brunken RC, et al (1989) Regional myocardial oxygen consumption determined noninvasively in human with [1–^{11}C]acetate and dynamic positron tomography. Circulation 80:863–872

Arora R, Ferrick KJ, Nakata T, et al (2003) I-123 MIBG imaging and heart rate variability analysis to predict the need for an implantable cardioverter defibrillator. J Nucl Cardiol 10:121–131

Aruva MR, Daviau J, Sharma SS, et al (2006) Imaging thromboembolism with fibrin-avid ^{99m}Tc-peptide: evaluation in swine. J Nucl Med 47:155–162

Banati RB (2003) Neuropathological imaging: in vivo detection of glial activation as a measure of disease and adaptive change in the brain. Br Med Bull 65:121–131

Barron HV, Lesh MD (1996) Autonomic nervous system and sudden cardiac death. J Am Coll Cardiol 27:1053–1060

Basken NA, Mathias CJ, Lipka AE, et al (2008) Species Dependence of the [^{64}Cu]Cu-Bis(thiosemicarbazone) radiopharmaceutical binding to serum albumins. Nucl Med Biol 35:281–286

Ben-Haim S, Israel O (2006) PET/CT for atherosclerotic imaging. QJ Nucl Med Mol Imaging 50:53–60

Bengel FM, Schachinger V, Dimmeler S (2005) Cell-based therapies and imaging in cardiology. Eur J Nucl Med Mol Imag 32:S404–S416

Berman DS, Shaw LJ, Hachamovitch R et al (2007) Comparative use of radionuclide stress testing, coronary artery calcium scanning, and noninvasive coronary angiography for diagnostic and prognostic cardiac assessment. Semin Nucl Med 37:2–16

Berridge MS, Nelson AD, Zheng L et al (1994) Specific beta-adrenergic receptor binding of carazolol measured with PET. J Nucl Med 35:1665–1676

Bing RJ (1954) The metabolism of the heart. In: Harvey Society of NY (ed) Harvey lecture series. Academic, New York

Botker HE, Bottcher M, Schmitz O et al (1997) Glucose uptake and lumped constant variability in normal human hearts determined with [^{18}F]fluorodeoxyglucose. J Nucl Cardiol 4:125–132

Brinkmann JF, Abumrad NA, Ibrahimi A et al (2002) New insights into long-chain fatty acid uptake by heart muscle: a crucial role for fatty acid translocase/CD36. Biochem J 367:561–570

Brooks P, Clark R, Cheresh D (1994) Requirement of vascular integrin alpha v beta 3 for angiogenesis. Science 264:569–571

Buckman BO, Van Brocklin HF, Dence CS et al (1994) Synthesis and tissue distribution of [omega-^{11}C]palmitic acid. A novel PET imaging agent for cardiac fatty acid metabolism. J Med Chem 27:2481–2485

Carmeliet P (2000) Mechanisms of angiogenesis and arteriogenesis. Nat Med 6:389–395

Carrio I (2001) Cardiac neurotransmission maging J Nucl Med 42:1062–1076

Davies JR, Rudd JHF, Weissberg PL, et al (2006) Radionuclide imaging for the detection of inflammation in vulnerable plaques. J Am Coll Cardiol 47:C57–68

Delforge J, Syrota A, Lancon JP et al (1991) Cardiac betaadrenergic receptor density measured in vivo using PET, CGP12177, and a new graphical method. J Nucl Med 32:739–748

Dilsizian V, Bateman TM, Bergmann SR, et al (2005) Metabolic imaging with beta-methyl-p-[(123)I]-iodophenyl-pentadecanoic acid identifies ischemic memory after demand ischemia. Circulation 112:2169–2174

Dobrucki LW, Sinusas AJ (2005) Cardiovascular molecular imaging. Semin Nucl Med 35:73–81

Elsinga PH, van Waarde A, Vaalburg W (2004) Receptor imaging in the thorax with PET. Eur J Pharmacol 499:1–13

Falk E (2006) Pathogenesis of atherosclerosis J Am Coll Cardiol 47:C7–C12

Freundlieb C, Hock A, Vyska K (1980) Myocardial imaging and metabolic studies with [17–^{123}I]iodoheptadecanoic acid. J Nucl Med 21:1043–1050

Fuster V, Corti R, Fayad et al (2003) Integration of vascular biology and magnetic resonance imaging in the understanding of atherothrombosis and acute coronary syndromes J Thromb Haemost 1:1410–1421

Fuster V, Moreno PR, Fayad ZA et al (2005) Atherothrombosis and high-risk plaque part I: evolving concepts. J Am Coll Cardiol 46:937–954

Geng YJ, Libby P (1995) Evidence for apoptosis in advanced human atheroma. Am J Pathol 147:251–266

Goldstein DS, Eisenhofer G, Dunn BB et al (1993). Positron emission tomographic imaging of cardiac sympathetic innervation using 6-[^{18}F]fluorodopamine: initial findings in humans. J Am Coll Cardiol 22:1961–1971

Gould KL, Lipscomb K, Hamilton GW (1974) Physiologic basis for assessing critical coronary stenosis: instantaneous flow response and regional distribution during coronary hyperemia as measures of coronary flow reserve. Am J Cardiol 33: 87–94

Gropler RJ, Siegel BA, Geltman EM (1991) Myocardial uptake of carbon-11-acetate as an indirect estimate of regional myocardial blood flow. J Nucl Med 32:245–251

Heineman FW, Balaban RS (1993) Effects of after load and heart rate on NAD(P)H redox state in the isolated rabbit heart. Am J Physiol Heart Circ Physiol 264:H433–H440

Higuchi T, Wester HJ, Schwaiger M (2007) Imaging of angiogenesis in cardiology. Eur J Nucl Med Mol Imaging 34:S9–S19

Huisman MC, Higuchi T, Reder S et al (2008) Initial characterization of an ^{18}F-labeled myocardial perfusion tracer J Nucl Med 49:630–636

Imamura Y, Ando H, Mitsuoka W, et al (1995) Iodine-123 metaiodobenzylguanidine images reflect intense myocardial adrenergic nervous activity in congestive heart failure independent of underlying cause. J Am Coll Cardiol 26:1594–1599

Jain D (1999) Technetium-99 m labeled myocardial perfusion imaging agents. Semin Nucl Med 29:221–236

Jaffer FA, Weissleder R (2004) Seeing within: molecular imaging of the cardiovascular system. Circ Res 94:433–445

Jaffer FA, Libby P, Weissleder R (2006) Molecular and cellular imaging of atherosclerosis. Emerging applications. J Am Coll Cardiol 47:1328–1338

Kietselaer BL, Reutelingsperger CP, Heidendal GA, et al (2004) Noninvasive detection of plaque instability with use of radiolabeled annexin A5 in patients with carotid-artery atherosclerosis. N Engl J Med 350:1472–1473

Kline RC, Swanson DP, Wieland DM et al (2001) Myocardial imaging with I-123-metaiodobenzylguanidine. J Nucl Med 22:129–132

Knapp FF Jr, Ambrose KR, Goodman MM (1986a). New radioiodinated methyl-branched fatty acids for cardiac studies. Eur J Nucl Med 12:S39–S44

Knapp FF Jr, Goodman MM, CallahanAP, et al (1986b) Radioiodinated 15-(p-iodophenyl)-3,3-dimethylpentadecanoic acid: a useful new agent to evaluate myocardial fatty acid uptake. J Nucl Med 27:521–531

Knickmeier M, Matheja P, Wichter T, et al (2000) Clinical evaluation of no-carrieradded meta-(^{123}I)iodobenzylguanidine for myocardial scintigraphy. Eur J Nucl Med 3:302–307

Knight LC (1990) Radiopharmaceuticals for thrombus detection. Semin Nucl Med 20:526

Knight LC (1993) Scintigraphic methods for detecting vascular thrombus. J Nucl Med 34:554–561

Knight LC (2001) Radiolabeled peptide ligands for imaging thrombi and emboli. Nucl Med Biol 28:515–526

Knight LC (2003) Non-oncologic applications of radiolabeled peptides in nuclear medicine. Q J Nucl Med 47:279–91

Kotzerke J, Glatting G, van den Hoff J, et al (2001) Validation of myocardial blood flow estimation with nitrogen-13 ammonia PET by the argon inert gas technique in humans. Eur J Nucl Med 28:340–345

Krivokapich J, Huang SC, Selin CE et al (1987) Fluorodeoxyglucose rate constants, lumped constant, and glucose metabolic rate in rabbit heart. Am J Physiol 252:H777–H787

Kudo T (2007) Metabolic imaging using PET. Eur J Nucl Med Mol Imaging 34:S49–S61

Kyuma M, Nakata T, Hashimoto A, et al (2004) Incremental prognostic implications of brain natriuretic peptide, cardiac sympathetic nerve innervation, and noncardiac disorders in patients with heart failure. J Nucl Med 45:155–163

Landini L, Santarelli MF, Positano V, et al (2005) Molecular imaging: its application in cardiovascular diagnosis. Curr Pharm Des 11:2225–2234

Laudano AP, Doolittle RF (1978) Synthetic peptide derivatives that bind to fibrinogen and prevent polymerization of fibrin polymers. Proc Natl Acad Sci U S A 75:3085–3089

Lautamäki R, Tipre D, Bengel FM et al (2007) Cardiac sympathetic neuronal imaging using PET Eur J Nucl Med Mol Imaging 34:S74–S85

Lees RS, Lees AM, Strauss HW (1983) External imaging of human atherosclerosis. J Nucl Med 24:154–156

Libby P (2002) Inflammation in atherosclerosis. Nature 420:868–874

Liedtke AJ (1981) Alterations of carbohydrate and lipid metabolism in the acutely ischemic heart. Prog Cardiovasc Dis 23:321–336

Lin JW, Sciacca RR, Chou RL et al (2001) Quantification of myocardial perfusion in human subjects using ^{82}Rb and wavelet-based noise reduction. J Nucl Med 42:201–208

Lopaschul GD, Stanley W (1997) Glucose metabolism in the ischemic heart. Circulation 95:415–422

Lu E, Wagner WR, Schellenberger U, et al (2003) Targeted in vivo labeling of receptors for vascular endothelial growth factor: approach to identification of ischemic tissue. Circulation 108:97–103

Machac J (2005) Cardiac positron emission tomography imaging. Semin Nucl Med 35:17–36

Madar I, Ravert HT, Du Y, et al (2006) Characterization of uptake of the new PET imaging compound 18F-fluorobenzyl triphenyl phosphonium in dog myocardium. J Nucl Med 47: 1359–1366

Matter CM, Wyss MT, Meier P, et al (2006) ^{18}F-Choline images murine atherosclerotic plaques ex vivo. Arterioscler Thromb Vasc Biol 26:584–589

Merlet P, Delforge J, Syrota A, et al (1993). Positron emission tomography with [^{11}C]CGP - 12177 to assess beta-adrenergic receptor concentration in idiopathic dilated cardiomyopathy. Circulation 87:1169–1178

Muller JE, Abela GS, Nesto RW, et al (1994). Triggers, acute risk factors and vulnerable plaques: the lexicon of a new frontier. J Am Coll Cardiol 23:809–813

Muller JE, Tawakol A, Kathiresan S et al (2006) New opportunities for identification and reduction of coronary risk: treatment of vulnerable patients, arteries, and Plaques. J Am Coll Cardiol 47:C2–C6

Münch G, Nguyen N, Nekolla S et al (2000). Evaluation of sympathetic nerve terminals with ^{11}C-epinephrine and ^{11}C-hydroxyephedrine and positron emission tomography. Circulation 101:516–523

Naghavi M, Libby P, Falk E et al (2003) From vulnerable plaque to vulnerable patient. A call for new definitions and risk assessment strategies: part I. Circulation 108:1664–1672

Naghavi M, Falk E, Hecht HS, et al (2006) From vulnerable plaque to vulnerable patient–Part III: Executive summary of the screening for heart attack prevention and education (SHAPE) task force report. Am J Cardiol 98(2A):2H–15H

Nitzsche EU, Choi Y, Czernin J, et al (1996) Noninvasive quantification of myocardial blood flow in humans. A direct comparison of the [^{13}N]ammonia and the [^{15}O]water techniques. Circulation 93:2000–2006

Opie LH, Owen P (1975) Assessment of myocardial free NAD + /NADH ratios and oxaloacetate concentrations during increased mechanical work in isolated perfused rat heart during production or uptake of ketone bodies. Biochem J 148:403–415

Phelps ME, Huang SC, Hoffman EJ et al (1979) Tomographic measurement of local cerebral glucose metabolic rate in humans with (F-18)2-fluoro-2-deoxy-D-glucose: validation of method. Ann Neurol 6:371–388

Poe ND, Robinson GD Jr, Zielinski FW (1977) Myocardial imaging with ^{123}I-hexadecenoic acid. Radiology 124:419–24

Raffel DM, Wieland DM (2001) Assessment of cardiac sympathetic nerve integrity with positron emission tomography. Nucl Med Biol 28:541–559

Rosenpire KC, Haka MS, Jewett DM et al (1990). Synthesis and preliminary evaluation of ^{11}C-meta-hydroxyephedrine: a false neurotransmitter agent for heart neuronal imaging. J Nucl Med 31:1328–1334

Ross R (1999) Atherosclerosis–an inflammatory disease. N Engl J Med 340:115–126

Rudd JH, Warburton EA, Fryer TD, et al (2002). Imaging atherosclerotic plaque inflammation with [^{18}F]-fluorodeoxyglucose positron emission tomography. Circulation 105:2708–2711

Sanz J, Fayad ZA (2008) Imaging of atherosclerotic cardiovascular disease. Nature 451:953–957

Schaèfers M, Riemann B, Levkau B et al (2002) Current status and future applications of cardiac receptor imaging with positron emission tomography Nucl Med Commun 23:113–115

Schafers M, Riemann B, Kopka K, et al (2004) Scintigraphic imaging of matrix metalloproteinase activity in the arterial wall in vivo. Circulation 109:2554–2559

Schelbert HR (2004) Positron emission tomography of the heart: methodology, findings in the normal and disease heart, and clinical applications. In: Phelps ME (ed) PET: molecular imaging and its clinical applications. Springer, New York

Schön HR, Schelbert HR, Robinson et al (1982) C-11 labeled palmitic acid for the noninvasive evaluation of regional myocardial fatty acid metabolism with positron-computed tomography. I. Kinetics of C-11 palmitic acid in normal myocardium. Am Heart J 103:532–547

Schwaiger M, Bengel FM (2003) From thallium scan to molecular imaging. Mol Imaging Biol 4:387–398

Sciacca RR, Akinboboye O, Chou RL et al (2001) Measurement of myocardial blood flow with PET using 1–^{11}Cacetate. J Nucl Med 42:63–70

Sinusas AJ, Zaret BL (1995) Coronary artery disease. In Wagner HN, Szabo Z, Buchanan JW (eds): Principles of Nuclear Medicine, ed 2, Saunders, Philadelphia, Saunders

Sokoloff L, Reivich M, Kennedy C et al (1977) The [^{14}C]deoxyglucose method for the measurement of local cerebral glucose utilization: theory, procedure, and normal values in the conscious and anesthetized albino rat. J Neurochem 28:897–916

Spagnoli LG, Bonanno E, Sangiorgi G et al (2007) Role of inflammation in atherosclerosis. J Nucl Med 48:1800–1815

Stone CK, Pooley RA, DeGrado TR et al (1998) Myocardial uptake of the fatty acid analog 14-fluorine-18-fluoro-6-thia-heptadecanoic acid in comparison to beta-oxidation rates by tritiated palmitate. J Nucl Med 39:1690–1696

Strauss HW, Harrison K, Langan J.K, et al (1975) Thallium-201 for myocardial imaging. Relation of thallium-201 to regional myocardial perfusion. Circulation 51:641–645

Strauss HW, Grewal RK, Pandit-Taskar N (2004) Molecular imaging in nuclear cardiology Semin Nucl Med 34:47–55

Su H, Spinale FG, Dobrucki LW, et al (2005) Noninvasive targeted imaging of matrix metalloproteinase activation in a murine model of postinfarction remodeling. Circulation 112:3157–3167

Taillefer L (2001) Radiolabeled peptides in the detection of deep venous thrombosis. Semin Nucl Med 31:102–123

Taki J, Matsunari I (2007) Metabolic imaging using SPECT Eur J Nucl Med Mol Imaging 34:S34–S48

Tamaki N, Magata Y, Takahashi N et al (1992) Myocardial oxidative metabolism in normal subjects in fasting, glucose loading and dobutamine infusion states. Ann Nucl Med 6:221–228

Tamaki N, Morita K, Kuge Y et al (2000) The Role of Fatty Acids in Cardiac Imaging. J Nucl Med 41:1525–1534

Taylor M, Wallhaus TR, Degrado TR et al (2001) An evaluation of myocardial fatty acid and glucose uptake using PET with [^{18}F]fluoro-6-thia-heptadecatnoic acid and [^{18}F]FDG in patients with congestive heart failure. J Nucl Med 42:55–62

Thakur ML, Pallela VR, Consigny PM, et al (2000) Imaging vascular thrombosis with ^{99m}Tc-labeled fibrin α-chain peptide. J Nucl Med 41:161–168

Tillisch J, Brunken R, Marshall R et al (1986) Reversibility of cardiac wall-motion abnormalities predicted by positron tomography. N Engl J Med 314:884–888

Travin MI and Bergmann SR (2005) Assessment of myocardial viability. Semin Nucl Med 35:2–16

Tseng H, Link JM, Stratton JR et al (2001) Cardiac receptor physiology and its application to clinical imaging: present and future. J Nucl Cardiol 8:390–409

Vaidyanathan G, Zhao XG, Strickland DK, et al (1997) No-carrier-added iodine-131-FIBG: evaluation of an MIBG analog. J Nucl Med 38:330–334

Vallabhajosula S, Fuster V (1997) Atherosclerosis: imaging techniques and the evolving role of nuclear medicine. J Nucl Med 38:1788–1796

Vallabhajosula S, Machac J, Knesaurek K et al (1995) Imaging atherosclerotic lesions by PET using [^{18}F]fluorodeoxyglucose (FDG): preclinical studies in hypercholesterolemic rabbits. Circulation 92: 313

Virmani R, Burke AP, Farb F et al (2006) Pathology of the vulnerable plaque J Am Coll Cardiol 47:C13–C18

Yamamoto Y, de Silva R, Rhodes CG (1996) Noninvasive quantification of regional myocardial metabolic rate of oxygen by $^{15}O_2$ inhalation and positron emission tomography. Circulation 94:808–816

Yamashina S, Yamazaki J-I (2007) Neuronal imaging using SPECT. Eur J Nucl Med Mol Imaging 34:S62–S73

Wallhaus TR, Taylor M, DeGrado TR et al (2001) Myocardial free fatty acid and glucose use after carvedilol treatment in patients with congestive heart failure. Circulation 103: 2441–2446

Weissberg PL (2004) Noninvasive imaging of atherosclerosis: the biology behind the pictures. J Nucl Med 45:1974–1795

Wieland DM, Swanson DP, Brown LE et al (1979) Imaging the adrenal medulla with an I-131-labeled antiadrenergic agent. J Nucl Med. 20:155–158

Wieland DM, Brown LE, Rogers WL et al (1981) Myocardial imaging with a radioiodinated norepinephrine storage analog, J Nucl Med 22:22–31

Wolters SL, Corsten MF, Reutelingsperger PM et al (2007) Cardiovascular molecular imaging of apoptosis Eur J Nucl Med Mol Imaging 34:S86–S98

Wu JC, Yla-Herttuala S (2005) Human gene therapy and imaging: cardiology. Eur J Nucl Med Mol Imaging 32: S346–S357

Wu JC, Tseng JR, Gambhir SS (2004) Molecular imaging of cardiovascular gene products. J Nucl Cardiol 11:491–505

Wu JC, Bengel FM, Gambhir SS (2007) Cardiovascular molecular imaging. Radiology 244:337–355